

QATAR UNIVERSITY

COLLEGE OF ENGINEERING

RIGOROUS SIMULATION AND OPTIMIZATION OF THE COLD SECTION IN A
REAL LNG PLANT: UPFRONT NITROGEN REMOVAL AS PROCESS ENHANCING
CONCEPT

BY

HAJER MKACHER

A Thesis Submitted to
The College of Engineering
in Partial Fulfillment of the Requirements for the Degree of
Masters of Science in Environmental Engineering

January 2023

© 2023. Hajer Mkacher. All Rights Reserved.

COMMITTEE PAGE

The members of the Committee approve the Thesis of
Hajer Mkacher defended on 10/07/2022.

Prof. Fares AlMomani
Thesis/Dissertation Supervisor

Prof. Bassim Hameed
Thesis/Dissertation Co-Supervisor

Prof. Fares AlMomani
Committee Member

Dr. Ahmed Massoud Abdou
Comittee Member

Approved:

Khalid Kamal Naji, Dean, College of Engineering

ABSTRACT

MKACHER, HAJER, Masters : January : 2023,

Masters of Science in Environmental Engineering

Title: Rigorous Simulation and Optimization of the Cold Section in Real LNG Plant: Upfront Nitrogen Removal as Process Enhancing Concept

Supervisor of Thesis: Fares, AlMomani.

The global demand for LNG is expected to continue increasing over the next decades. Qatar, as one of the largest LNG exporters with a 22% global share, announced in 2020 a plan to increase the production capacity by more than 60% over the next five years. The LNG industry relies on the liquefaction process to reduce the volume of natural gas (NG) by approximately 600 times. NG liquefaction offers a cost-effective way of transportation in tanks instead of relying on a network of pipelines for gas transportation.

NG processing and liquefaction include complicated unit operations such as impurities removal (e.g. CO₂, H₂S), separation of heavy hydrocarbons (C³⁺), and then liquefaction. The cold section is the pillar of the liquefaction process and consumes roughly 60% of the total energy demand. This section is comprised of the refrigeration cycles (C₃MR or SMR, etc.), fractionation unit, nitrogen removal unit (NRU), and helium extraction unit. Shaft work used to operate compressors accounts for the majority of the total energy demand in this section. Therefore, heat integration and process optimization are commonly used to reduce energy demand in the LNG process

This thesis aims to establish an effective upfront nitrogen removal (UN_{rem}) process in the hope to save energy, improve efficiency, increase production, and boosting the economic feasibility. This novel idea was validated via rigorous simulation of the cold section process using Aspen HYSYS® integrated with Aspen EDR® operated. Energy

optimization, detailed exergy analysis, and economic analysis for several UN_{rem} cases were conducted and compared.

Results showed that the total power requirement and the production rate can be decreased upon the implementation of the UN_{rem} concept. Compared with baseline operation, removing up to 87.5% of nitrogen from the feed was found optimal as it decreases the total power requirement by 0.24 MW and increases the LNG product flow rate by 4.4 %, while exergy loss decreased by 7.08 MW. UN_{rem} of 87.5% scenarios showed a profit of 24.2 billion USD in 20 years. Results confirmed the importance of UN_{rem} process for energy savings, process improvement, and profit without the need for structural changes.

DEDICATION

Dedicating to my family for their endless support.

ACKNOWLEDGMENTS

Throughout this thesis work, I have received great support from my entourage and my colleagues. First, I would like to thank my supervisor Prof. Fares AlMomani and Prof. Bassim Hameed for their guidance during the writing of the dissertation. Second, I would like to thank Dr.Essa Almosleh for his continuous support and patience in the early stages of this thesis. I would like to acknowledge my colleague Ajinkya Pal for his help in this work. His help and assistance in sections related to process optimization and simulation are highly acknowledged. Finally, I am very grateful for my family and their moral support that gives me the strength to work and achieve what I have done so far.

TABLE OF CONTENTS

DEDICATION	v
ACKNOWLEDGMENTS	vi
LIST OF TABLES	ix
LIST OF FIGURES	x
ABBREVIATIONS	xi
CHAPTER 1: INTRODUCTION	1
1.0. Background	1
1.1. NG and LNG Demand	1
1.2. LNG and Energy	3
1.3. Objectives	5
1.4. Thesis outline	6
CHAPTER 2: LITERATURE REVIEW	7
2.1. Review	7
2.2. Conclusion	12
CHAPTER 3: PROCESS DESCRIPTION	14
CHAPTER 4: RIGOROUS SIMULATION OF COLD SECTION	18
4.1. Introduction	18
4.2. Methodology	19
4.3. Results and Discussion	20
CHAPTER 5: PARAMETRIC OPTIMIZATION OF UPFRONT NITROGEN REMOVAL	26

5.1. Introduction	26
5.1.1. Description of Optimization Algorithm.....	26
5.1.2. Decision Variables	27
5.2. Upfront Nitrogen Removal Concept	28
5.3. Methodology	29
5.4. Results and Discussion.....	34
CHAPTER 6: EXERGY ANALYSIS OF UPFRONT NITROGEN REMOVAL.....	44
6.1. Methodology	44
6.2. Results and Discussion.....	45
CHAPTER 7: TECHNOLOGIES USED FOR UPFRONT NITROGEN REMOVAL	
.....	48
7.1. Introduction	48
7.2. Techniques of nitrogen capture from NG	49
CHAPTER 8: ECONOMIC ANALYSIS OF UPFRONT NITROGEN REMOVAL	57
8.1. Introduction	57
8.2. Methodology	59
8.3. Results and discussion.....	64
CONCLUSIONS AND RECOMMENDATIONS	72
REFERENCES	74

LIST OF TABLES

Table 4-1: Design data and specifications	20
Table 4-2: Overall Geometrical Summary of Heat Exchangers in the cold section.	21
Table 4-3: Fins characteristics of the MSHEs	24
Table 5-4: PSO parameters used in the optimization.....	31
Table 5-5: Scenarios of upfront nitrogen removal (UN_{rem})	31
Table 5-6: Boundaries of decision variables.....	33
Table 5-7: Optimal results of decision variables of all scenarios	35
Table 5-8: Results of optimized C_3MR compressors' total energy consumption in all scenarios.....	37
Table 5-9: Results of optimization in different nitrogen removal scenarios.	38
Table 6-10: Exergy Results for the base case and scenario 8	47
Table 8-11: Cost Estimates Classes [77, 78]	58
Table 8-12: Correlation constants for equipment	60
Table 8-13: Relations used for the OPEX estimate	62
Table 8-14: Molar flows of inlet and outlet streams in removal technology.....	63
Table 8-15: Parameters used for the lithium cycle capital cost estimation.....	64
Table 8-16: Profit of UN_{rem} technology with the lithium cycle for 20 years.....	70

LIST OF FIGURES

Figure 1-1: Changes in fuel consumption in industry from 2019 to 2030 [4]	2
Figure 1-2: Global LNG demand from 2018 to 2025 [1]	3
Figure 1-3: Power Consumption for LNG supply sections in MW[7]	5
Figure 3-4: Block Flow Diagram of Cold Section studied	17
Figure 4-5: Schematic of layers in MSHEs	23
Figure 5-6:Schematic diagram of conventional LNG cold section	28
Figure 5-7:Schematic diagram of the upfront nitrogen removal scenario	29
Figure 5-8: Flowchart of the PSO algorithm applied to the process.....	32
Figure 6-9: Exergy Diagram for the base case.....	45
Figure 6-10: Exergy Diagram for 87.5% UNrem	46
Figure 8-11: The overall CAPEX and OPEX for the cold section in all UN _{rem} scenarios	65
Figure 8-12: Distribution of CAPEX cost in scenario 7 among the process equipment	66
Figure 8-13: Share of OPEX parameters in scenario-7	67
Figure 8-14: LNG sale revenue over 20 years for the UN _{rem} scenarios.....	68
Figure 8-15: CAPEX and OPEX of removal technique for UN _{rem} scenarios.....	69
Figure 8-16: Ammonia sales for the UN _{rem} scenarios	70

ABBREVIATIONS

NG	Natural Gas
NGL	Natural Gas Liquid
Mtoe	Mega Tonnes of oil equivalent
NRU	Nitrogen Removal Unit
SRU	Sulfur Removal Unit
C ₃ MR	propane and Mixed Refrigerant
SMR	Single Mixed Refrigerant
MOFs	Metal-Organic Frameworks
PAFs	Porous Aromatic Frameworks
CMS	Carbon Molecular Sieves
GHG	Green House Gases
MMM	Mixed Matrix Membranes
DOF	Degree of Freedom
MW	Molecular Weight
MCHE	Main Cryogenic Heat Exchange
PSO	Particle Swarm Optimization
RVP	Reid Vapor Pressure
SPC	Specific Power Consumption
EFG	End Flash Gas
AACE	American Association of Chemical Engineering
PFD	Process Flow Diagram
USD	United States Dollar

CHAPTER 1: INTRODUCTION

1.0. Background

1.1. NG and LNG Demand

After the Paris agreement in 2015 to limit the temperature increase to 1.5 C by 2050 and satisfy net-zero emissions by 2055-2080 [1], the world's attention is directed to natural gas as a source of clean energy. LNG has proven to be more environmentally friendly than any other fossil fuel, as it generates 44% less CO₂, 81% less CO, and 80% less NO_x per energy unit in comparison to oil and coal [2]. With these environmental benefits, the consumption of NG has increased to satisfy the need of the different industrial sectors. Figure 1-1 depicts the changes in fuel type for supplying various industries such as chemicals, aluminum, and cement in Mtoe. It can be observed that the use of coal and oil as fuel sources has declined dramatically in all industries. Whereas, renewables, natural gas, and electricity demand have increased. NG is mostly used in the light chemical industries with energy demand in the range of 80 to 90 Mtoe as well as industry iron/steel sector with an energy demand of 30 Mtoe. [3] This helps to explain the continuous increase in the demand for NG.

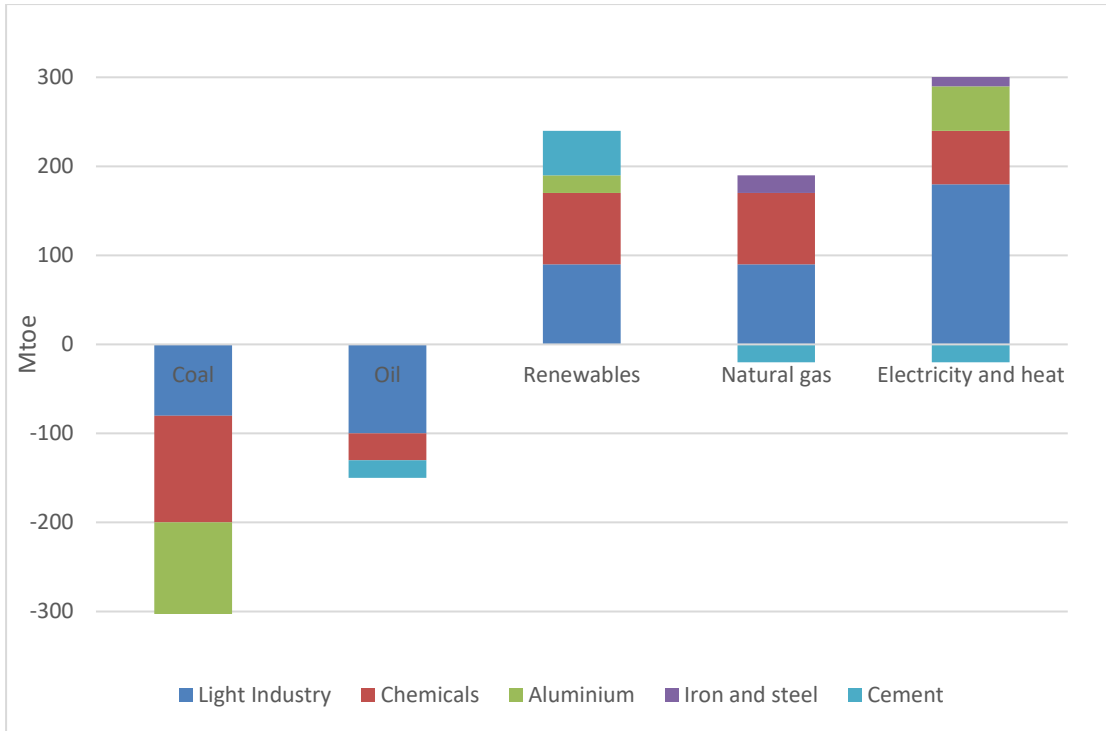


Figure 1-1: Changes in fuel consumption in industry from 2019 to 2030 [4]

In general, the NG industry relies on the liquefaction process to reduce its volume by approximately 600 times. liquefied natural gas (LNG) offers a cost-effective way of transportation in tanks instead of relying on a network of pipelines for gas transportation.[5] [6].

Qatar as the largest LNG exporter with a share of 22% of global production in 2020 has announced to increase its LNG production by over 60% for the next 5 years.[7] The global demand is predicted to be increased up to 22.2% in 2025 compared to 2020. Figure 1-2 represents the global LNG supply throughout the years 2018 to 2025. [1] Data reveals that the demand would increase from 390 million metric tons in 2021 to 450 million metric tons in 2025. As the LNG supply chain consists of a series of compression, liquefaction, and cooling stages that are energy-intensive. The application

of novel technologies and optimization strategies to optimize the LNG process would reduce power consumption and increase the process's economic feasibility.

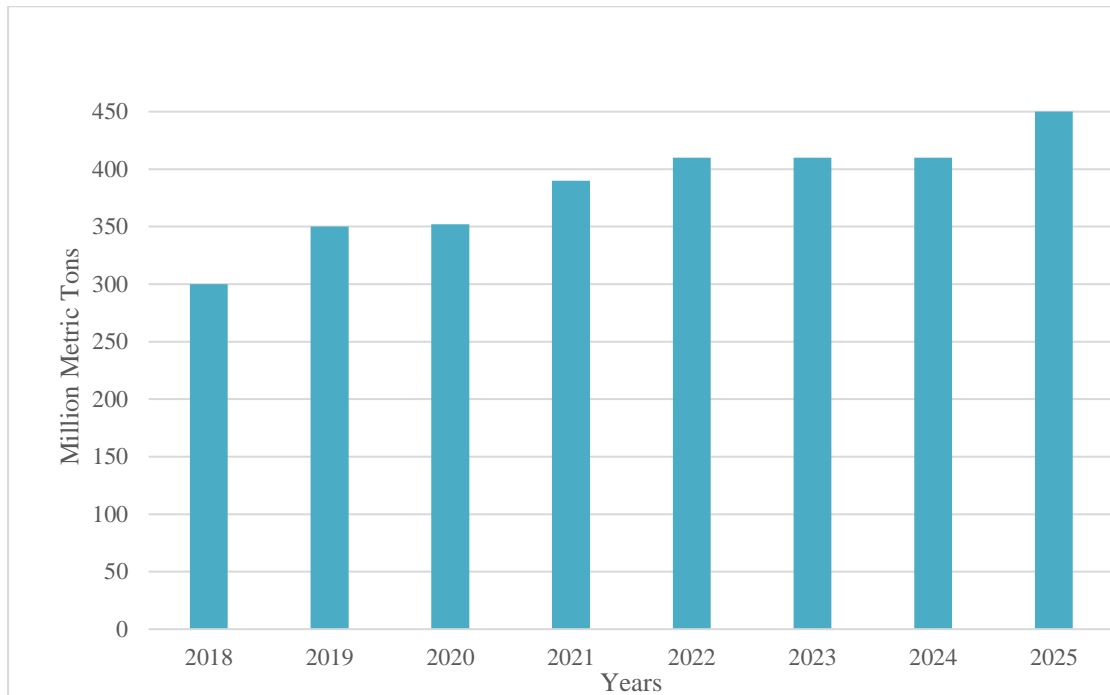


Figure 1-2: Global LNG demand from 2018 to 2025 [1]

1.2. LNG and Energy

The NG processing and liquefaction include complicated unit operations such as impurities removal (e.g. CO₂, H₂S, He, N₂, H₂O, and Hg), separation of heavy hydrocarbons (C³⁺), and then liquefaction. Within the LNG plant, the cold section is the pillar of the liquefaction process and consumes roughly 60% of the total energy demand. This section is comprised of the refrigeration cycles (C3MR or SMR, etc.), fractionation unit, nitrogen removal unit (NRU), and helium extraction unit. The shaft work required to run the compressors accounts for the majority of the total energy

demand in this section. Therefore, the cold section is considered the most energy-intensive because it required a very low temperature for NG liquefaction, high specific energy to operate compressors, and extensive cooling of refrigerants utilities. Consequently, heat integration and process optimization are commonly used to reduce energy demand in the LNG process. It was estimated that the total energy consumed in the cold section can reach up to 99.57 MW for the LNG production rate of 20477 kmol/h [7] refrigerants cycles and compressors within the liquefaction stage require up to 860 kJ/kg and 2.9 MJ/kg, respectively. [8]

Figure 1-3 presents the detailed power requirements for an actual LNG supply chain. The lowest power demands in the LNG process are the sulfur removal unit, sweetening section, pre-separation, and NGL with 1.2 MW, 4.762 MW, 2.346 MW, and 0.037 MW, respectively. This power is generally used for compression, steam generation, and pumping. The power consumed in the nitrogen removal section and export of the terminals doesn't exceed 10 MW. Most of this power is used to operate pumps. Obviously, the liquefaction process has the highest power consumption of 121.1 MW. This energy is used to operate a series of compressors, refrigerant cycle intercoolers, and pumps.

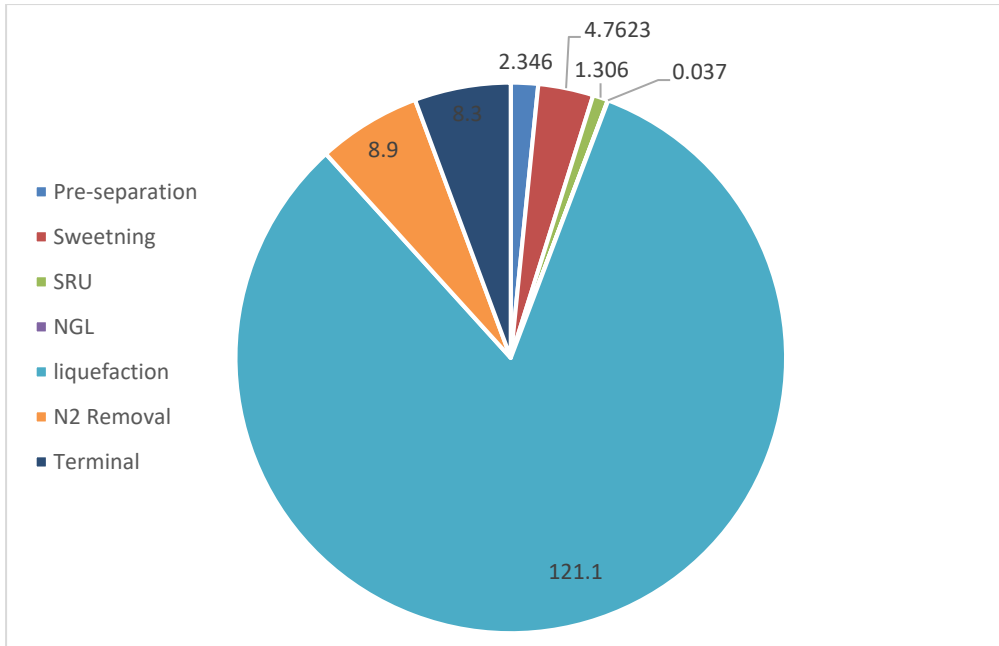


Figure 1-3: Power Consumption for LNG supply sections in MW[7]

As previously said, increasing the LNG production rate to meet the expanding demand for fuel would increase the amount of energy required for liquefaction, resulting in additional costs. Therefore, there is a crucial need for new approaches and alterations that could be incorporated into the cold section to reduce its energy demand and keep the operation profitable. Such improvements should comply with the process conditions with no major changes in the supply chain.

1.3. Objectives

To meet rising worldwide NG demand, it is critical enhancing LNG output while keeping the same process structure using less power. Therefore, the objective of this thesis is to achieve a profitable and sustainable LNG liquefaction process without the need for radical structural changes in the supply chain. To achieve this objective, the thesis was structured in two parts: the first part deals with developing, for the first time, a complete simulation process of the liquefaction unit (i.e the cold section). The uniquely developed simulation process, which mimics a real LNG liquefaction unit in

Qatar, allows for studying a wide range of alternatives to optimize the production rate and energy requirement of the process. In this part, detailed designs of all the unit operations in the cold section were prepared and calibrated based on real plant conditions. The second part involves investigating the effect of removing nitrogen before the cold section (i.e. upfront nitrogen removal) on the power consumption, cost, and production rate of the process. Removing nitrogen before the cold section would decrease the energy required to liquify the NG and allow for production increment to replace the removed nitrogen

1.4. Thesis outline

This thesis is divided into 8 chapters. Chapter 1 presents a brief overview of NG and LNG consumption stating the objectives to be achieved. Chapter 2 shows the work done in the literature regarding LNG simulation, power optimization of the liquefaction section, and the upfront nitrogen removal with a critical evaluation of the literature deficiencies. Chapters 3 and 4 include process description and simulation of the real liquefaction section in the LNG supply chain. Chapters 5 and 6 present the optimization and the exergy analysis of the upfront nitrogen removal methodology and results respectively. Chapter 7 shortlist the different technologies used for upfront nitrogen removal with their advantages and drawbacks on nitrogen- hydrocarbons separation. The last chapter is the techno-economic analysis of the optimized cold section with UN_{rem} .

CHAPTER 2: LITERATURE REVIEW

This chapter aims to summarize the work done on LNG process enhancement and optimization methods to decrease the power consumption of the liquefaction section in the LNG process.

2.1. Review

The increase in LNG production is accompanied by an increase in energy consumption, as the liquefaction process consumes about 60 % of the total power of the LNG plant. [9]. The shaft work required to run the process compressors accounts for the majority of the total energy demand in this section. As a result, heat integration and process optimization are commonly used to reduce energy demand in the LNG process.

Different Research works focused on optimizing these units to minimize energy consumption and increase the process's economic feasibility. Lee et al.[10] investigated standalone and integrated NRU processes for varying nitrogen content in NG feed. The study showed that the process integration could decrease the specific energy requirements by 38.6% in comparison to the base process. Additionally, it was highlighted that the energy requirement in the process depends on the mass fraction of nitrogen in the feed, and concluded that standalone NRU is favorable for nitrogen fractions below 17 mole %. In addition, they compared the results of energy consumption while having an end-flash drum or stripping column in producing LNG. Results are dependent on the mass fraction of nitrogen in the feed. However, this study is limited by a specific nitrogen content in the feed gas which cannot be applied to other processes. Another method of decreasing the power consumption in the cold section is the rearrangement and replacement of other equipment in the process. Ghorbani, Hamed et al [11] suggested an integrated system of LNG, NGL, and NRU that reduces the plant size and the total specific power from 19.5% to 24% compared to the original

configuration. The study relied on solar energy to operate compressors work which can be deflected by the weather and thus decreases process efficiency. On the other hand, Eterafi, Gorjian et al [12] suggested implementing an absorption refrigeration cycle using ammonia instead of the C₃MR and DMR for cooling utility; this method has reduced the consumption by about 18.4% and 12.6%. Chen, Okasinski et al [13] suggested another pathway for high-energy efficiency in the LNG cold section by optimizing the NRU section. Nonetheless, there is no research work or studies that explored the effect of nitrogen removal before the cold section on process efficiency, production rate, and energy requirements.

Pal, Al-Musleh et al [14] presented the results of single and double-column integrated NRU in the cold section. The double-column NRU shows a specific power reduction of 5.5% compared to the base case and a 4.8% reduction in total power requirement compared to the single column. The cost of the changes in types of equipment is not considered. Obviously, the work done on the energy optimization did not take into consideration the effect of feed gas components on the energy consumption for the cold section, the cost of each method, and the applicability of these techniques in actual industries. A scattered search algorithm with NLP solver gradient-based is used for a system of different levels in the refrigeration cycle and for another system of refrigeration in a cascade where it gives a result of a 3% saving in energy consumption. [15] Another algorithm proposed is the knowledge-based algorithm which aims to find the optimum value of flowrates in the MR components, the lowest boiling point flowrate was increased (nitrogen in this case) and it concluded that even the pressure of the MR has a great increase on the compression power but also have given the opportunity to further decrease the MR flowrate. The optimization has resulted in a 13% of compression power reduction.[16, 17] For a mixed cascade process as a

refrigerant in an LNG plant, a multi-variate Coggins approach is used; where feed and ambient conditions for MR are changed to predict the energy loss. Results of 35.91 % decrease in energy loss with 25.4 % overall energy savings. This method was suitable for onshore applications. [18] The same method was done for another offshore application that aims to minimize the total liquefaction energy which in this way reduces the load on the C₃MR cycle and reduces its energy consumption. The energy has been reduced by 21.7%. [19] The combination of process enhancement and optimization algorithms resulted in a significant enhancement in efficiency by 61%. Although, the implementation of the genetic algorithm of type NSGAI two-objective for the optimization work does decrease the energy consumption by 3.7 % only, meaning that this method is not the best among other optimization processes. [20]

Usage of PSO as an algorithm for optimization is not common but recently researchers started to use it for different optimization aims. As an example, optimization of composite curves was done for the C₃MR cycle using the PSO algorithm using a surrogate-assisted modeling methodology. Results that the PSO algorithm overrates the GA algorithm for the same process and gives better results. [21]

The GA algorithm is exploited to optimize the NGL and LNG design integrated units. Mathematical analysis is done using the Design-Expert™. Selecting the compressors' outlet pressures and composition as the manipulated variables. After several iterations and retrofitting of the process to increase the ethane recovery, optimal numbers are extracted. The overall exergy efficiency of 53% is reached compared to the current plant state. [22] The same work was done in this paper using the same algorithm. The modeling was done using Aspen HYSYS™ and optimization work revealed a 23% reduction.[23]

Pham et Al [17] proposed two options of optimization that can be integrated to find the

best solution, finding the optimum composition of MR can affect energy efficiency, the refrigerant composition of N₂, C₁, C₂, C₃, isobutene, and Iso-pentane temperature were adjusted to have the best heat exchange. After finding optimal value, the second option of optimization is applied, where the rearrangement of the process was needed, booster compressor as added along with heavy refrigerant components. The energy was saved up to 53.8 % in the power consumption through this combination of changes. Not only composition is changed but also the MR and the C₃ compressor pressure can have a great impact on energy consumption. Pimabudi et Al [24] worked on maximizing the efficiency of the cycle and also cost-saving. Using Aspen plus™ and GA in Matlab™ has saved 71% of investment cost and exergy efficiency by 61 %. [24]

Heat transfer is the most important factor for this concern, other researchers have suggested changing the type of the heat exchangers in the liquefaction process from multi-stream plate-fin to brazed plate. The effect of these changes has been studied these changes were studied through the genetic algorithm that shows a reduction of 14.7 % in the total exergy loss.[25] Exergy analysis is important and algorithms are the most useful methods to do that, researchers have developed their algorithm as an example, hybrid modified coordinate descent to decrease the energy used for the mixed refrigerant in the LNG process. After modeling with hysys, the process shows a reduction of 44.3 % [26] In the same way, exergy analysis was done through the integration between hysys and Matlab™ using the GA method for maximizing the C3MR cycle efficiency in the LNG process and for minimizing the product utilization. Simultaneous optimization work was done which gives a result of a 15 % reduction. [27] Ghorbani et Al have used the same method but simultaneous energy and cost optimization are studied. First, pinch analysis is conducted to find the highest value of exergetic energy and then compared with the results of coding optimization. [28]

The type of refrigerant is important as different heat loads are accompanied by different refrigerants. The number of components in the MR composition is studied where up to six components are chosen from 84 possible combinations. The behavior of different combinations is compared and discussed concerning the MCHE energy. Composite curves show that the high boiling components increase the heat flow in the MCHE. Thus, it has to be removed for better heat transfer. [29] Wang et al [30] suggested mixing propane with iso-butane as a refrigerant and to be compared with the C₃-MR cycle efficiency. First, the energy consumption of the C₃MR refrigerant is calculated using the simulation then the mixture was changed to C₃C₄-MR and optimized using GA. The exergy of the system with the new refrigerant has decreased to 28.5%. A certain condition should be maintained for this system which is the heat load that should not exceed 60 %; otherwise, a liquid phase will be entering the compressor.[30] Sanavandi and Ziabasharhagh [31] worked on optimizing the refrigerant composition in the C₃MR refrigeration by considering operational constraints. Initially, the specific energy consumption was 1028.94 kJ/kg and decreased to 973.93 kJ/kg. The study didn't consider the applicability of the method in the industry plus the cost aligned with these changes.

Simpler methods were followed for the optimization which is setting the objective function which is the power consumption and finding the different parameters to change, trial and error is done by changing values of propane and MR inlet pressure, MR expansion pressure, inlet flow for each refrigerant each time with a certain range and check the effect of this change of the power values. Results show that the variation in the inlet flow has the greatest effect on the power produced, which has decreased to 30% compared to initial values. [32]

Others have done a rigorous process simulation using HYSYS and then applied a two-

level operation system, the first for minimizing energy losses and the second for a self-optimizing control. The DOF has been studied and control variables have been set. The methane mole fraction, the temperature, and the suction pressure of the compressors have shown a great impact on energy losses. [33] The system with the changing variables has saved 259.7 kJ/kg- LNG. The results show that the control system of the process has a greater impact on efficiency more than the changes that can be made after the implementation of the plant. Another method is using the embedded optimization method called “BOX “in the Aspen hysys software for two processes which are the C3MR cycle and the C3MR with split propane. Both systems were operating under the same conditions. By optimizing the temperature, pressure, and composition of the refrigerant; results show that both UA of heat exchangers and the refrigerant flow rate have a great impact up to 28 % reduction. [34] From multiple simulations, the best optimization variable for the cycle is the temperature difference, Using steady-state optimality analysis, this paper has only proven that this variable is the most suitable variable that affects the C3MR cycle energy consumption at different MR flowrates, this was proven through the analysis of T-S diagrams for C3MR cycle. [35]

2.2. Conclusion

Previous work was done on minimizing the energy consumption of compressors in exemplary LNG processes. Although, none has worked on an actual plant model that makes results more realistic, and also the optimization methods were limited to certain constraints that give a local minimum solution within the search space. The PSO algorithm used for this research results in the global best solution for the unconstrained optimization problem. Moreover, research is not focused on the effect of feed components such as nitrogen on the liquefaction energy consumption in the cold section. To show the importance of upfront nitrogen removal, this thesis work will provide a quantitative analysis of upfront nitrogen removal in terms of energy and

production. The idea of removing nitrogen from the feed stream consists of installing a removal process prior to the cold section, where the feed gas will be processed with no nitrogen fraction. For solid and realistic results, a rigorous simulation of the cold section is done based on the actual LNG plant and actual operating conditions. For the first stage, several cases of nitrogen removal are studied in terms of energy consumption and LNG product flow rate. Later on, the optimization of the process is executed taking the benefit of refrigerants cooling capacity with maintaining the high purity product and HHV within the international specification. Clearly, none of the cited research has taken into consideration the LNG HHV value which represents the main buyer's focus. These constraints would need a process retrofitting or changes in operating conditions depending on the fraction of upfront nitrogen removed.

CHAPTER 3: PROCESS DESCRIPTION

Figure 3-4 presents the cold section in the base case of the LNG process, which comprises the NGL recovery unit, liquefaction, NRU, helium extraction unit, propane pre-cooled mixed refrigerant (C₃MR) cycle, and fractionation. As this thesis focuses on the refrigeration cycle and nitrogen removal, the simulation of fractionation is excluded. The mixed refrigerant (MR) stream (S-133) undergoes three stages of compression along with interstage cooling. S-133 is compressed and condensed at three pressure levels of low (1.6 bar), medium (2.98 bar), and high (5.09 bar) in K-100, K-101, and K-102 respectively. Compression at each stage is followed by cooling the MR stream in water coolers with a minimum temperature approach of 5°C. Before entering the main cryogenic heat exchanger (HE-104), MR is pre-cooled from 42°C (S-102) to -31°C (S-134) in the propane cycle which is represented in brown color. As the legend represented; the brown and green arrows are utilized to represent streams associated with propane and mixed refrigerant cycles respectively. The high-pressure MR streams (S-136 and S-138) are cooled in HE-104, before undergoing Joule-Thompson expansion to provide requisite cold energy. Similar to the MR cycle, the propane cycle also consists of three stages of compression. The propane stream at 1.5 bar (S-147) is compressed to 2.89 bar, 5.09 bar (S-149), and 16.62 bar (S-151) in K-103, K-104, and K-105 respectively. S-151 is cooled in X-104 and is throttled to provide requisite cold energy to pre-cool the MR and pre-treated dry natural gas (S-100) stream.

The stream S-100 enters the chiller (E-100) and the propane cycle, where it is cooled from 21°C to -27°C (S-104). S-104 is throttled to the operating pressure (54 bar) of the NGL recovery unit (C-100) using V-100. The rapid expansion further cools the NG stream (S-105) to -45°C and also reduces the heat load on the MR cycle. S-105 enters C-100, which produces light overhead vapor (S-106) and heavy bottoms liquid (S-107)

streams. The stream S-107 is further heated in X-100 and undergoes phase separation in R-100 to generate a reboiler vapor stream (S-108), which returns to the bottom stage of C-100. The liquid stream (S-109) of R-100 makes up the NGL product. The stream S-109 is at 80°C and 54.94 bar and is further directed to the fractionation unit. The light overhead vapor stream, S-106 at -36°C, is directed to the main cryogenic heat exchanger (HE-104) and cooled to produce S-110 at -54°C. S-110 undergoes phase separation in the reflux drum (R-101) and the condensed NG (S-112) returns to C-100. The vapor from the R-101 (S-111) is liquefied in HE-104 to produce S-113 at -144°C. The requisite cold energy for the liquefaction is sourced by evaporating low-pressure MR streams (S-142 and S-146). The stream S-113 is mixed with the methane-rich stream (S-115) from the fractionation unit to produce S-116, which is then directed to HE-104 to further sub-cool the stream and produce S-117.

To satisfy the final LNG product specifications, stream (S-117) is directed to the nitrogen removal unit (NRU) and helium extraction units. First, the product (S-117) is throttled using a pressure valve (V-103) from 16.37 bar to 5.96 bar then phase-separated in R-102. The overhead stream from R-102 is rich in helium (S-118) and it enters the crude auto flash helium heat exchanger (HE-105) to be cooled from -140°C to -181 °C (S-120). Then, it is directed to the crude helium separator (R-103) that rejects up to 80% of helium. The overhead of the separator (S-121) is used as a cooling utility in HE-105, and the outlet stream (S-125) leaves at -148°C. The percentage mole fraction of helium in stream S-123 was set at 58% as per industrial specifications. Similarly, the bottom stream (S-122) of R-103 is also used as a cooling utility for HE-105, after throttling in V-104 from 5.86 bar to 1.81 bar. The stream S-122 is heated from -182°C to -147°C in HE-105. To meet the specified nitrogen content in the LNG product, the extra nitrogen in the bottom stream of R-102 (S-119) is removed using a stripping

column (C-102). Therefore, stream S-119 is cooled from -144°C to -155°C in HE-106 to form S-126. The stream S-126 is then throttled across V-105 from 5.77 bar to 1.61 bar before entering C-102. A side stream (S-126) source from stage-2 of C-102, provides the cooling in HE-106 and returns to the bottom stage of C-102 as a reboiler stream (S-129).

The overhead of C-102 is mixed with stream S-124 to form the fuel gas stream S-131, which is further used to condensate the MR vapor (S-137) in the fuel gas/MR heat exchanger (HE-107) This process results in a nitrogen rejection of 88%. The bottom stream from C-102 is the LNG product (S-128) ready for storage.

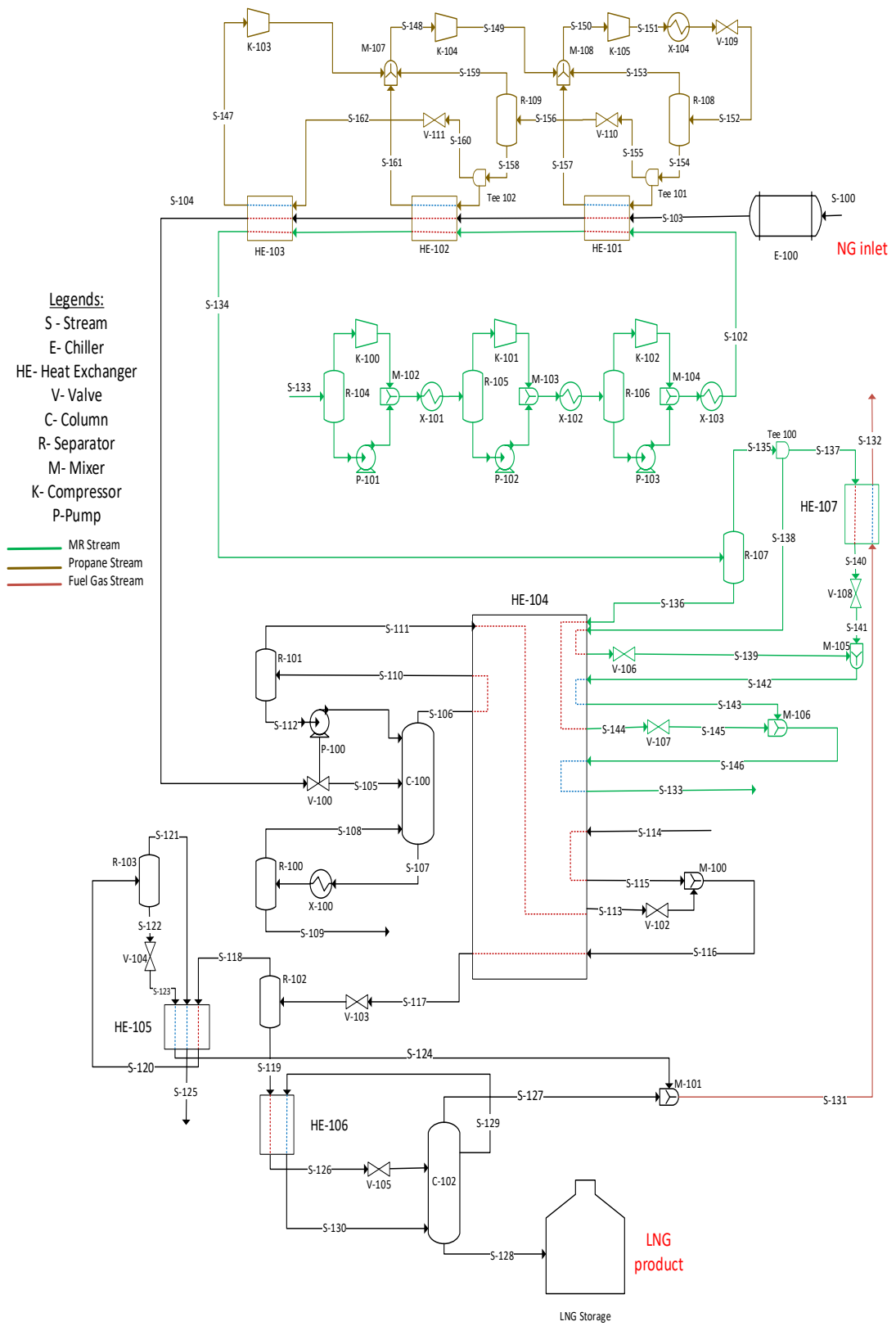


Figure 3-4: Block Flow Diagram of Cold Section studied

CHAPTER 4: RIGOROUS SIMULATION OF COLD SECTION

This chapter aims to present the importance of conducting a rigorous simulation of the cold section for more realistic results and a tunable process. The methodology followed and the results obtained are presented as well.

4.1. Introduction

The internal designs of process equipment play an important role in improving the output of a chemical process. Models always rely on the operation conditions and the specifications of the desired product to get the optimum design that guarantees the optimal equipment efficiency. The physical details of equipment help to understand the behavior and to predict the performance for better qualification. Thus, to obtain a flexible process that handles all possible changes, the simulation of the cold section in this thesis is done rigorously based on an existing LNG baseload. This section describes the methodology followed for the internal models' simulation of heat exchangers in the LNG cold section. Heat exchanger internal design is performed in a way that satisfies the heat transfer surface, conductance, and total length.[36] All heat exchangers simulated are plate fin-type, which were picked carefully to achieve the required performance. The fins are mainly aimed to provide an extended heat transfer surface area. Four types of fins were used: plain, serrated, perforated, and herringbone. In all configurations, the fluid is directed in different ways for each. For the plain it is directed in straight horizontal rows, in perforated, it is directed through straight horizontal rows with holes, the serrated is represented by aligned compacted rectangles and herringbone is a series of zigzagged rows. These differences in configuration give the fins different thermohydraulic characteristics that may affect their performance. The fin's conditions in the heat exchange affect its performance, in which the fin coating should be taken into account since it affects the thermal insulation. As the thickness of the coating increases, more heat is lost and it shows a decreased performance for the heat

exchanger. This criterion should be taken into account during the manufacturing process to not decrease the fin efficiency. [37]

4.2. Methodology

The rigorous internal design of heat exchangers in the cold section is based on the actual operating conditions of the LNG plant. Streams were simulated using HYSYS™ software under specific operating conditions of inlet temperature, inlet pressure, and gas flow rate. Considering all these conditions, the EDR™ software executes a preliminary design that should be tuned to obtain the desired outlet temperature. Certain specifications mentioned in Table 4-1 are considered for the equipment design. It was important to maintain the desired outlet stream conditions and product quality while simulating the equipment. Essentially, the right number of layers, the distributor's axial length and the fins specifications (type, height, thickness, frequency) have the most impact on the stream's outlet temperature and pressure. The fin height is to define the distance between the separating plates and the frequency is to specify the number of fins per meter in the plate. The internal design of MCHE (HE -104), Helium heat exchanger (HE-105), nitrogen re-boiler (HE-106), and fuel gas heat exchanger (HE-107) are executed using stream-by-stream simulation with a plate-fin type.

The compressors in the C₃MR cycle were simulated using compressor curves which correlate the volumetric flow to the head and polytropic efficiency. Quadratic extrapolation was used to identify the required values. The off-design correction was specified at -12°C and 44.1°C for reference temperature and reference MW, respectively. Using these curves and the outlet pressures specified for each stage, the compressor speed and outlet temperature are calculated by the software. Compressed propane is being cooled from 66°C to 44°C using two seawater coolers. The seawater flow rate is adjusted depending on the desired outlet temperature. The cooled propane is divided into three propane evaporators. The flow ratio is calculated by the software

by defining the vapor fraction for the propane stream in evaporators. The flow fraction was calculated by the software based on the required phase of the steams. The pressure of streams is decreased using valves to have the same pressure as the outlet propane from the separators. The same work was done to simulate the MR cycle.

Table 4-1:Design data and specifications

Design Specification	Value
Compressor and Pump adiabatic efficiency, percentage	80
Tray efficiency, percentage	100
Number of stages in NGL recovery column	10
Number of stages for rectifying section in NRU column	15
Number of stages for stripping section in NRU column	15
Cooling water temperature, °C	40
Min temperature approach for cooling water heat exchanger, °C	5
LNG product pressure, Bar	1.2

4.3. Results and Discussion

Table 4-2 presents the detailed design information for all the equipment. The results of rigorous internal designs are obtained from EDR™ software and HYSYS™ for the HE-104, HE-105, HE-106, and HE-107. All exchangers are simulated and designed as plate-fin types. The metal type used for all exchangers is aluminum for its high thermal conductivity and resistance to low temperatures and different ranges of pressures.[38] The exchangers' designs varied following the change in heat exchange and heat flux.

The flow was directed upward as a better option for suitable outlet temperature. The type and height of fins in the heat exchanger were arranged to maintain the uniform heat exchange between and within the plates and achieve the required heating load.

Table 4-2: Overall Geometrical Summary of Heat Exchangers in the cold section.

	HE -104	HE-105	HE-106	HE-107
No. of 20	1	1	1	1
Exchangers in parallel				
No. of 1	1	1	1	1
Exchangers per unit				
No. of layers per exchanger	101	19	91	109
Core length (mm)	5857	2005.99	1407.06	725.17
Core width (mm)	886.7	128.59	1193.64	793.4
Core depth (mm)	931	149.6	682.4	600.8
Distributor length-end A (mm)	313.8	48.45	363.27	281.14

		HE -104	HE-105	HE-106	HE-107
Main heat transfer length (mm)		5230	1909.08	565	299.9
Distributor length-end B (mm)		313.8	48.45	478.79	144.13
Internal effective width (mm)		863.7	105.59	1170.64	770.4
Side bar width (mm)		11.5	11.5	11.5	11.5
Parting sheet thickness (mm)		2	1	1	1
Cap sheet thickness (mm)		5	5	5	5

Figure 4-5 shows the layer distribution of MSHE with distributors and inlet streams. HE-104 has seven layers of A, B, C, D, E, F, and G for the inlet streams from 1 to 8. The gray crossed boxes represent the distributors of each layer, white boxes are the inactive fins which has no flow. Layer A has an extra two elements from the typical layer sequence which are the redistributor outflow for a partial flow to the intermediate header, layer C has a redistributor inflow with a length of 244.34 mm that increase the

fraction of the inlet flow by taking the outflow from another layer using the header. The redistributor outflow was needed for layers D and G with an axial length of 225.45 mm and 302.3 mm respectively that partially direct the flow to the intermediate header. HE-105 has 3 streams which result in three layers A, B, and C. the internal configuration consists of a redistributor outflow in layer B with an axial length of 32.66 mm. HE-106 has two layers A and B with the typical arrangement of an inlet distributor of 351.77 mm in length, the main fin of 565 mm, an outlet distributor of 351.77 mm, and an end bar of 11.5 mm. Similarly, HE-107 has two layers A and B with an inlet distributor of 269.54 mm in length, the main fin of 300 mm, outlet distributor of 145.13 mm with an end bar of 0 mm.

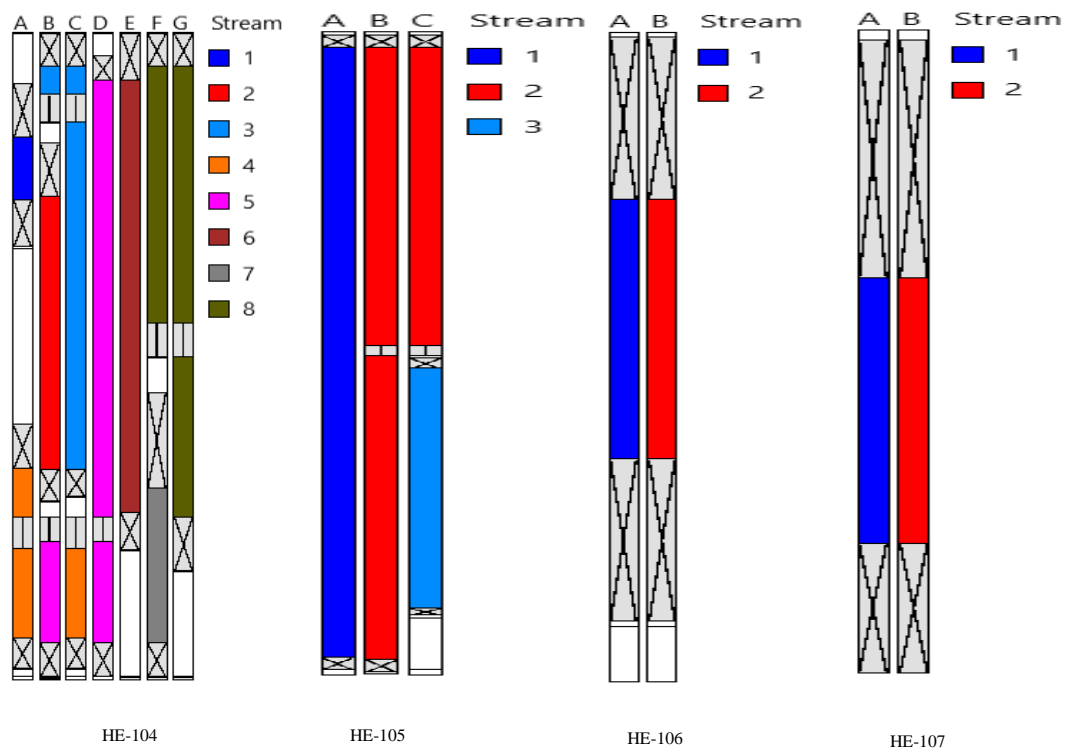


Figure 4-5: Schematic of layers in MSHEs

Table 4-3 shows the fin characteristics of each heat exchanger. The thickness and height of the fins in the heat exchanger are arranged to maintain the uniform heat exchange between and within the plates for the required heating load. The fin height for HE- 104/ 105/106 is 6.4 mm, which is the optimal value that cannot be exceeded, or else it will decrease the heat transfer and the temperature will be increased. Moreover, the pressure drop will also increase which is not a preferable situation in this case. [39] Fins height in the same stream should have the same height which is applied in fins 1 and 3 and fins 2 and 4 in HE-107 with a height of 10 mm and 1.2 mm respectively. These values are within the range provided by the software which is a minimum of 1.2 mm to 15 mm. Since fin thickness is important for thermal conductivity; the optimum fin thickness is between 0.2 mm and 0.9 mm. It can be noticed that the fin frequency of HE-106 is much lower than the other heat exchangers which are restricted by a range of 0 to 2 number/mm generated by the software because of the low-pressure drop specified for the heat exchanger. The type is selected upon the fin's heat transfer efficiency as mentioned earlier. Perforated and serrated was most used for the internal configuration because of their high efficiency and high heat transfer increase with a decreased pressure that is needed for the design.

Table 4-3: Fins characteristics of the MSHEs

		Type	Height (mm)	Thickness (mm)	Frequency (number/mm)
HE-104	Fin1	Plain	6.4	0.51	472
	Fin 2	Perforated	6.4	0.51	472
	Fin 3	Serrated	6.4	0.51	472
	Fin 4	(offset)	6.4	0.41	787
	Fin 5		6.4	0.3	787

		Type	Height (mm)	Thickness (mm)	Frequency (number/mm)
	Fin 6	Plain	6.4	0.41	787
HE-105	Fin1	Serrated	6.4	0.2	787
	Fin2	Perforated	6.4	0.2	787
	Fin3		6.4	0.2	787
HE-106	Fin1		6.4	0.2	0.787
	Fin2		6.4	0.2	0.787
	Fin3		6.4	0.2	0.236
HE-107	Fin1	Serrated	10	0.41	755
	Fin2	(offset)	1.2	0.3	755
	Fin3		10	0.9	755
	Fin4		1.2	0.9	755

CHAPTER 5: PARAMETRIC OPTIMIZATION OF UPFRONT NITROGEN REMOVAL

5.1. Introduction

5.1.1. Description of Optimization Algorithm

This section aims to optimize the C₃MR compressors by changing the refrigerant flow composition: nitrogen, methane, ethane, and propane for MR and C₃ streams. As a result, optimum power for compressors and minimum energy can be used. PSO is an effective method to optimize chemical processes with simple coding. Initially developed by James and Russell, [40] it depends on generating multiple solutions and iterations then choosing the best solution from a group of solutions, and then choosing the global optimum number that can be resulted. It shows a high ability to solve nonlinear objective functions in the black box software (eg.HYSYS™). The first step is the initialization of the particle, where a random velocity and position are set. A range of maximum and minimum values is given for the velocity as well as for the position which can tighten the particle's movements. Matlab™ starts to generate random numbers for the decision variables and iterate between numbers and plug it into the objective function until finding the best solution and updating it to the global best solution within the search space.[40]

Description of particle position is done using a vector x:

$$X = [x_1 + x_2 + x_3 + x_4] \quad \text{Equation 1}$$

The trajectory of each particle can be described by the equation of motion as:

$$x_i(t + 1) = x_i(t) + v_i(t + 1) \quad \text{Equation 2}$$

The updated velocity of the particles is described by:

$$v_i(t + 1) = v_i(t) + c_1(p_i - x_i(t))R_1 + c_2(g - x_i(t))R_2 \quad \text{Equation 3}$$

Where t is time, t+1 is the next iteration, v_i is the velocity component of the particle in

one dimension, p_i is the personal best that a particle reaches at a certain time, g is the global best that describes the best position of the particle in the swarm, c_1 and c_2 are the acceleration constants that specify the value of steps taken by the particle, R_1 and R_2 are two matrices that generate random variables that each is plugged until reaching the best and the global best position and velocity.

The first step in the algorithm is the problem definition where to specify the objective function, the decision variables, and the PSO parameters. The second step is the initialization of the swarm, where the position and the velocity of the particle are specified with the constraints of the search space that should be respected during the motion of the particles in the search space. The third step is the iteration of the particle position and velocity to find the personal best and the continuous update to result in the global best solution.

5.1.2. Decision Variables

Since PSO is used in the optimization process, decision variables should be specified. After the DOF study, many variables can be changed. In this case, the flow rates of nitrogen, methane, ethane, and propane are chosen to be changed continuously to find the optimum minimum power. The range is specified below and above the actual flow rates, it is changed each time for finding the global optimal value. A starting point has been selected to initialize the execution of the code which is called “initial population initialization”, the particle will be initiated with a random position and velocity as mentioned earlier within the upper and lower bond specified.

The objective function is: $P = \sum_i^{i+1} P_i$ Equation 4

With $i = [1,6]$

Where the P is the total power for MR and C_3 cycle

5.2. Upfront Nitrogen Removal Concept

Removing upfront nitrogen from the NG stream coming from the hot section in the LNG supply chain comes from the idea that the nitrogen does not contribute to the heating value of LNG. The nitrogen accompanied by hydrocarbons is undergoing cooling processes in the cold section. the liquefaction of nitrogen requires extensive cooling energy because of its low boiling point. As a result, to reduce the energy consumed, nitrogen should be removed before entering the cold section to not waste energy on liquefying its portion. To clarify the idea, Figure 5-6 shows the conventional LNG process diagram, where the NG from the hot section enters with 4.9 nitrogen mol % that undergoes all the precooling and liquefaction processes. The nitrogen removal unit removes almost 95% of the nitrogen in the NG stream. The conventional configuration shows that the nitrogen rejection unit is located after the NGL recovery and the liquefaction process.

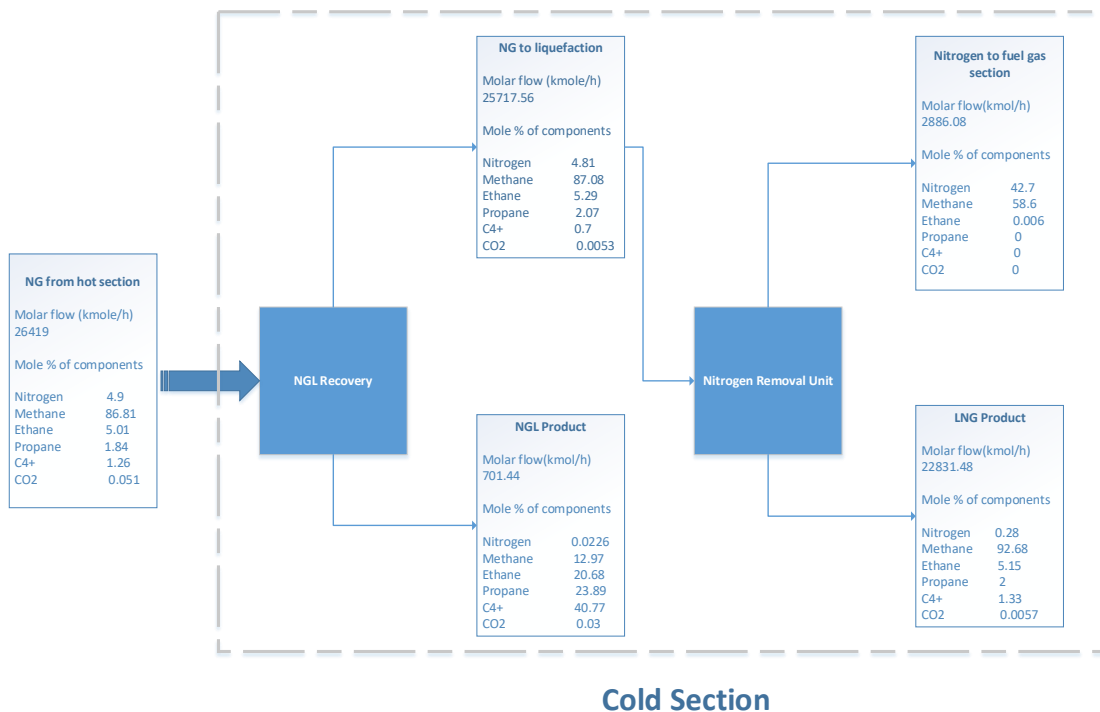


Figure 5-6: Schematic diagram of conventional LNG cold section

On the other hand, the scenario of removing upfront nitrogen would be represented in Figure 5-7 where to shift the nitrogen rejection section prior to the cold section. the removal efficiency can reach up to 85% using specified technology for removal. This new process configuration would reduce the energy consumed in the cold section. Calculations in the diagram are representative based on rough estimations and material balance just to justify the idea. Compared with Figure 5-6 it can be noticed that an extra LNG product of 12.27% can be obtained with the same feed flow rate of 26420.3 kmol/h and the same LNG product quality.

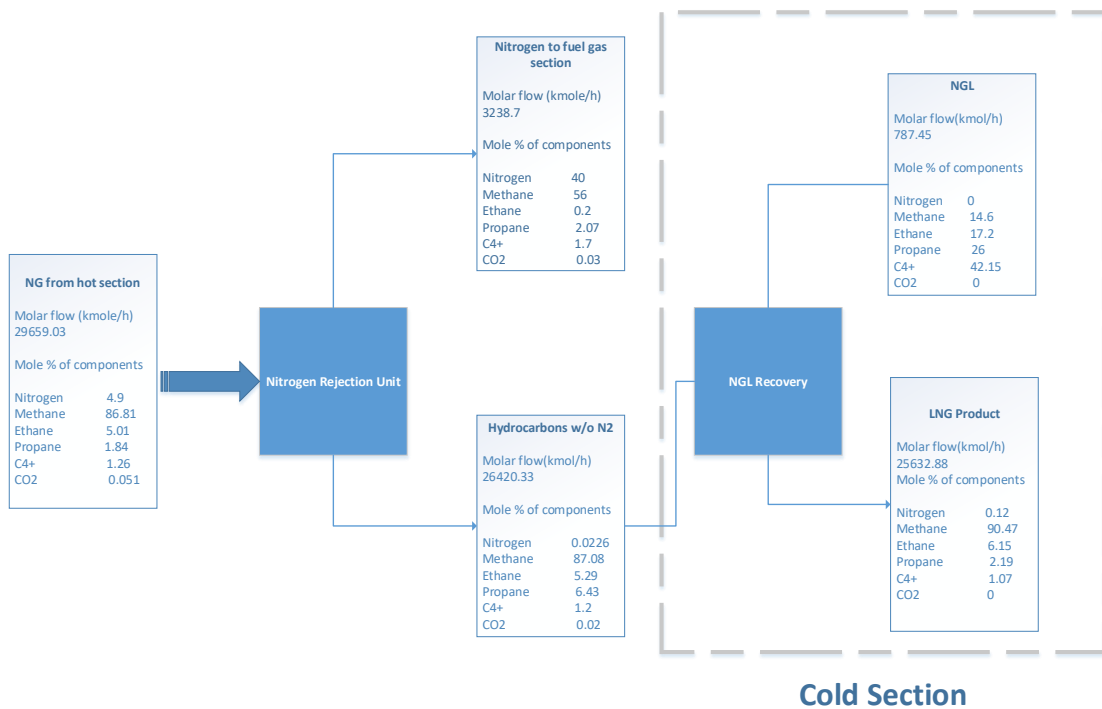


Figure 5-7: Schematic diagram of the upfront nitrogen removal scenario

5.3. Methodology

The idea of upfront nitrogen removal (UN_{rem}) focuses on rejecting the nitrogen

content present in dry gas by an additional process retrofitting. To satisfy the LNG product specification, operational conditions were tuned to maintain similar molar flowrate, LNG HHV, RVP of the NGL, and helium content. The temperature of the reboiler in the NGL column (C-100) and the S-110 temperature were changed to ensure more liquid in the scrub column and maintain the same flow rate of the produced NGL. The temperature of the effluent LNG from the HE 104 stream (S-117) was manipulated to achieve the required specification for the plant's final product (i.e. HHV of 1105 Btu/SCF). Once the constraints were established and stabilized, the optimization of the different scenarios of UN_{rem} is executed using the PSO algorithm. The seven scenarios of UN_{rem} studied in this thesis are presented in Table 5-5. The base case without UN_{rem} was optimized and used for comparison purposes. As shown in Figure 5-8, the first step is to specify the decision variables that the iteration will be based on, and also the constraints of the search space for the swarm. Hence, for this optimization, the MR component's flow rates, the pressure ratio of S-102, and MR temperatures (S-139 and S-144) are selected as decision variables since it has a direct effect on the energy consumption in the MR cycle. The PSO parameters used in the optimization under converging conditions are presented in Table 5-4. The inertia weight is specified for momentum particle control. Clerc and Kenedy constriction coefficients (κ , Φ_1 , and Φ_2) are specified as constrictions for the inertia coefficient specified before and for c_1 and c_2 in $v_i(t + 1) = v_i(t) + c_1(p_i - x_i(t))R_1 + c_2(g - x_i(t))R_2$ Equation 3. The Clerc and Kenedy equation is defined as:

$$\chi = \frac{2\kappa}{12 - \phi - \sqrt{\phi^2 - 4\phi}} \quad \text{Equation 5}$$

It states that the inertia coefficient (ω) = χ

$$c_1 = \chi \phi_1 \text{ and } c_2 = \chi \phi_2 \quad \text{Equation 6}$$

This will make the iteration tighter and more specific. [41] The damping factor is used

for an optimal global search in a large search space. The size of the particles and maximum iteration is also specified for the code execution. From a set of solutions, a maximum is picked and then a global maximum is selected concerning the set constraints. If the results are not satisfactory, the code generates a new number of solutions to be tested. At the end of the execution, the global maximum is selected where it provides the needed cooling effect without any losses.

Table 5-4: PSO parameters used in the optimization

Specification	Value
Inertia weight (ω)	0.729
kappa	1
Phi 1	2.05
Phi 2	2.05
Damping factor	0.99
Global acceleration factor	1.49
Personal acceleration factor	1.49
Particle size for each variable	50
Maximum iterations	100

Table 5-5: Scenarios of upfront nitrogen removal (UN_{rem})

Upfront Nitrogen Removal (%)	Description
0	Base Case
12.5	Scenario - 1

Upfront Nitrogen Removal (%)	Description
25	Scenario - 2
37.5	Scenario -3
50	Scenario - 4
62.5	Scenario -5
75	Scenario - 6
87.5	Scenario - 7

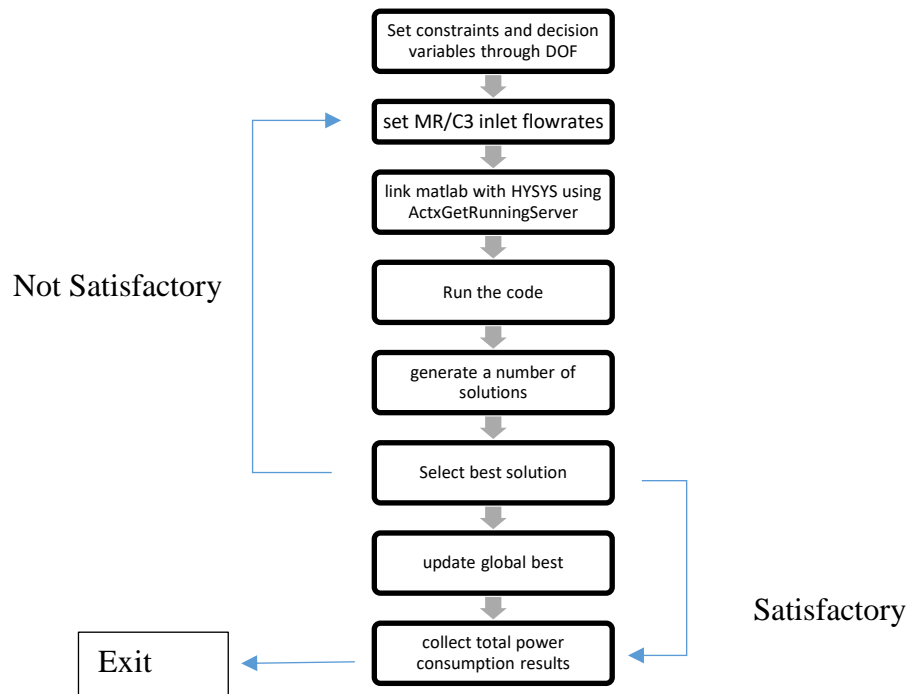


Figure 5-8: Flowchart of the PSO algorithm applied to the process

Table 5-6 presents the decision variables from x 1 to x11 with the description and range specified within the optimization. These variables were selected to be below and above the actual flow rates and were changed for each iteration to find the global optimal value. A starting point has been selected to initialize the execution of the code which is

called “initial population initialization”, the particle will be initiated with a random within the upper and lower bond specified.

Table 5-6: Boundaries of decision variables

Decision variables	Description	Stream	Range
x1 (Kg/s)	Nitrogen Flow Rate in MR	S-133	0-200
x2 (Kg/s)	Methane Flow Rate in MR	S-133	0-200
x3 (Kg/s)	Ethane Flow Rate in MR	S-133	0-200
x4 (Kg/s)	Propane Flow Rate in MR	S-133	0-200
x5 (Kg/s)	n- Butane Flow Rate in MR	S-133	0-200
x6 (Kg/s)	i-Butane Flow Rate in MR	S-133	0-200
x7 (Kg/s)	i-Pentane Flow Rate in MR	S-133	0-200
x8	Pressure Ratio		7-15 (17-38)
		S-102	
x9 (C)	Temperature MR lq out (C)	S-144	-130 to -100
x10 (C)	Temperature MR vap out (C)		-150 to -120
		S-139	
x11	Split ratio of Tee 100		0-0.5
		Tee-100	

The purity of the produced LNG was set at the global specification by carrying out iterations bounded by constraints specified in Equations 7 to 10:

$$\text{Temperature of SN} - 117 \leq \text{Temperature of liquefaction} \quad \text{MTA of}$$

$$\text{MSHE} \geq 2^{\circ}\text{C} \quad \text{Equation 8}$$

$$\text{MTA of MSHE} \geq 2^{\circ}\text{C} \quad \text{Equation 8}$$

$$\text{RVP of scrub column bottom (S - 107)} \geq 2040 \text{ psi} \quad \text{Equation 9}$$

$$\text{HHV of LNG product (S - 128)} \geq 1105 \text{ Btu/SCF} \quad \text{Equation 10}$$

Providing a suitable liquefaction temperature for the LNG stream with no wasted heat is an important factor that should be assured which is applied through Equation 7 and

Equation 10. The liquefaction temperature is reaching -145°C , which is the optimal temperature that assures the continuous production of liquids. (Equation 7). All the MTA range for MSHE is also constrained. (Equation 8) The removal of heavy hydrocarbons should respect the ethane fraction in the bottom NGL recovery (Equation 9) where the pressure should not exceed the baseline pressure. The most important specification for LNG is its caloric value where it is sold depending on this value, thus, the HHV of LNG product should not exceed its baseline value to maintain high quality. (Equation 10)

5.4. Results and Discussion

After the rigorous simulation of the liquefaction unit, the second step is to optimize the energy consumed in different UN_{rem} scenarios. The decision variables were based on total energy consumed and products specification.

Table 5-7: Optimal results of decision variables of all scenarios

Decision Variables	Base Case	Scenario-1	Scenario -2	Scenario-3	Scenario-4	Scenario-5	Scenario-6	Scenario-7
x1 (kg/s)	4.19	4.2	4.46	4.25	4.4	4.5	4.7	4.9
x2 (kg/s)	59.18	57.45	58.45	57.32	57.39	57.44	57.32	58.37
x3 (kg/s)	169.22	171.44	175.02	157.13	156.37	155.98	162.25	163.84
x4 (kg/s)	0	0	0	0	0	0	0	0
x5 (kg/s)	102.13	98.26	98.23	92.62	91.46	91.76	92.94	88.39
x6 (kg/s)	0.18	0.0	0.49	0	0	0	0	0
x7 (kg/s)	0.0	0.0	0.0	0	0	0	0	0
x8 (Bar) ^b	8.55 (21.6)	8.6 (21.75)	8.72 (22.06)	8.92 (22.56)	9.1 (23.23)	9.2 (23.27)	9.25 (23.40)	9.3 (23.52)
x9 (C)	-118.05	-122.20	-122.66	-123.58	-121.03	-121.70	-124.93	-122.74
x10 (C)	-144.72	-144.07	-145.37	-144.83	-146.04	-145.93	-145.58	-147.67
x11 (C)	0.05	0.05	0.04	0.04	0.04	0.04	0.04	0.03

^b The pressure value is presented instead of the pressure ratio.

The optimal results for the decision variables (x_1 to x_{11}) for all UN_{rem} scenarios are presented in Table 5-7. In addition, it shows the optimal pressure and temperatures for a successful liquefaction process that varies around $-122 \pm 2^\circ\text{C}$, and 8.2 ± 0.2 Bar respectively. It can be noticed that as the percentage of nitrogen removal increases from 12.5% to 87.5% the required pressure increases from 8.55 bar to 9.2 bar. This trend is related to the fact that a high nitrogen fraction as a light component requires higher pressures.[16] It was noticed that some variables such as propane and i-pentane flow rates do not have any effect on the performance of the refrigeration cycle for all removal scenarios. However, the i-butane can have a significant effect on percentage removal in the range of 12.5% to 25% with an optimal flow rate that does not exceed 0.49 kg/s. For other refrigerants' components like n-butane and I-butane optimal flow rates increase in most scenarios of removal. All is depending on the specific refrigeration effect on the dominant components as the nitrogen is removed.

Table 5-8: Results of optimized C₃MR compressors' total energy consumption in all scenarios

		Base Case	Scenario-1	Scenario-2	Scenario-3	Scenario-4	Scenario-5	Scenario-6	Scenario-7
Description	Component	Power (MW)							
MR Cycle	K-100	18.50	18.60	18.69	18.57	18.60	18.70	18.85	18.86
	K-101	20.24	20.35	20.46	20.40	20.49	20.60	20.76	20.80
	K-102	21.69	21.81	21.97	22.55	22.79	22.93	22.94	23.32
	P-101	0.02	0.03	0.03	0.00	0.01	0.01	0.00	0.01
	P-102	0.03	0.03	0.03	0.01	0.01	0.01	0.02	0.02
	P-103	0.03	0.03	0.03	0.02	0.02	0.02	0.02	0.01
Total		60.52	60.85	61.20	61.55	61.92	62.27	62.60	63.02
C₃ Cycle	K-103	7.94	7.81	7.67	7.87	7.76	7.62	7.35	7.34
	K-104	13.60	13.47	13.42	13.15	13.02	12.87	12.75	12.77
	K-105	17.00	16.85	16.73	16.43	16.25	16.13	16.10	15.70
Total		38.54	38.14	37.82	37.45	37.02	36.62	36.20	35.81
Other	P-101	0.00040	0.00041	0.00039	0.00044	0.00037	0.00042	0.00036	0.00041
Components									

	Base Case	Scenario-1	Scenario-2	Scenario-3	Scenario-4	Scenario-5	Scenario-6	Scenario-7
Total Power Requirement (MW)	99.57	99.50	99.54	99.53	99.47	99.42	99.36	99.33

Table 5-9: Results of optimization in different nitrogen removal scenarios.

	Base Case	Scenario-1	Scenario-2	Scenario-3	Scenario-4	Scenario-5	Scenario-6	Scenario-7
LNG Product mass flow rate (MTPA)	3.47	3.48	3.51	3.52	3.56	3.58	3.61	3.63
Pressure (Bar)	1.20	1.20	1.20	1.20	1.20	1.20	1.20	1.20
Temperature (°C)	-160.20	-160.03	-159.98	-159.84	-159.87	-159.80	-159.75	-159.63

	Base Case	Scenario-1	Scenario-2	Scenario-3	Scenario-4	Scenario-5	Scenario-6	Scenario-7
Nitrogen content (mol%)	0.20	0.15	0.14	0.12	0.11	0.11	0.12	0.10
HHV (Btu/Scf)	1105.00	1105.00	1105.00	1105.00	1105.00	1105.00	1105.00	1105.00
NGL Molar flow rate (kmol/h)	530.35	531.70	530.31	531.67	530.66	531.26	530.77	531.10
Pressure (Bar)	54.94	54.94	54.94	54.94	54.94	54.94	54.94	54.94
Temperature (°C)	80.00	80.27	80.20	85.50	80.35	80.91	80.51	81.20
RVP (psia)	2042.00	2041.00	2041.09	2041.09	2040.58	2040.46	2042.11	2041.56
Total Power Requirement (MW)	99.57	99.50	99.54	99.53	99.47	99.42	99.36	99.33

	Base Case	Scenario-1	Scenario-2	Scenario-3	Scenario-4	Scenario-5	Scenario-6	Scenario-7
SPC	28.70	28.57	28.34	28.26	27.91	27.80	27.55	27.38
(MW/MTPA)								

Table 5-8 shows the energy optimization results for the compressors and pumps in the C₃MR cycle and other components in the cold section unit for all nitrogen removal scenarios. It can be noticed that the energy consumption of the MR increased from 60.52 MW to 63.02 MW for the scenario corresponding to 87.5% of UN_{rem} compared with the base case. This increase is due to the increase of hydrocarbons in the gas stream as a replacement for the removed nitrogen, which would need more energy to be liquefied at higher pressures. It can be further explained through Table 5-9 **Error! Reference source not found.**, where the required pressure in the scenario of 87.5% Nitrogen is the highest ~9.3 Bar compared with other scenarios because as removing nitrogen more hydrocarbons are present that needed higher cold energy to be liquefied, thus the MR should be compressed to a higher pressure. In the propane cycle and other components, the power decreases by 7% and 2% respectively as the nitrogen content decreases. Since it is executed at a lower pressure, it becomes easy to cool and less energy is consumed. However, the total power required, despite the increase in MR cycle energy consumption, was decreased by increasing the percentage of nitrogen removed due to the decrease of power requirement in the propane cycle and other components. Compared to the base case, it can be recorded that the total power requirement decreases from 99.57 MW to around 99.54 ± 0.01 MW in the case of 12.5%, 25%, and 37.5% UN_{rem}. In addition, it decreases by around 99.42 ± 0.6 MW in the case of 50%, 62.5%, and 75% of UN_{rem}. The major decrease is recorded in the case of removing 87.5% upfront nitrogen, which was by a percentage of 0.241 %. The SPC represents the total power requirement over the LNG flow rate and shows a decrease of 4% when 87.5% of N₂ is removed compared to the base case. It was concluded that the more volatile components are present in the gas stream; the more compression power. Thus, with the removal of nitrogen, the total power required decreases.

Table 5-9 shows the optimized temperature, pressure, HHV, and RVP for the LNG and NGL units that were selected as constraints. The product mass flowrate was fluctuating around 3.52 ± 0.07 MTPA with all nitrogen removal scenarios suggesting minimal production problems. The pressure and temperature of the LNG product for all scenarios were kept at 1.2 bar and -159°C . These two parameters were stabilized for the NGL product at 54 bar and 80°C . It was noticed that increasing the percentage of nitrogen removal stabilized the HHV for LNG and RVP for the NGL and marinated within the required specifications. The increase in percentage nitrogen removal was combined with an increase in product mass flow by 4 % compared to the base, which means that the UN_{rem} creates an extra capacity for hydrocarbon processing. Under optimum UN_{rem} the power consumption in the LNG plant decreased from 123 MW to 99.57 MW. For further results illustration, the SPC, which represents the total power requirement over the LNG product flow rate, was calculated for all UN_{rem} scenarios. There was a decrease of 4% in the case of removing 87.5% of upfront nitrogen compared to the base case. This proves that the fraction of methane, ethane, propane, I-butane, N- butane, and I-pentane affects the power consumed in the C_3MR cycle. These results can be taken into consideration for a more profitable plant without the need for a radical structural change in plant design. During the optimization work, it was observed that after the removal of 75% of nitrogen the NRU column is not required and can be replaced by a simple vessel. To avoid structural modification which cannot be applied to an exciting plant design; the effluent LNG product (S-117) from the HE-104 was subcooled from -144°C to -147°C and flashed in R-102 to maintain the same product specifications as mentioned before. The process of removing nitrogen from dry gas can be applied right after the pretreatment process. The feed gas entering the cold section will be free from any nitrogen content that will provide extra hydrocarbon flow

rates with less energy consumed.

Work Contribution:

Hajer: Introduction, Description, Methodology Results analysis

Ajinkya: The code, the optimization (SBO)

CHAPTER 6: EXERGY ANALYSIS OF UPFRONT NITROGEN REMOVAL

6.1. Methodology

The exergy concept was applied around the base case and the proposed nitrogen removal process to identify the exergy loss; that is the total exergy destroyed in the system as a result of irreversibilities. The exergy loss is could be calculated by implementing exergy balance around the desired control volume. Exergy is transferred across a system in three forms: mass flow, heat, and work. Thus, the exergy balance of an open steady-state system can be expressed in the most general form as follows:

$$\sum_{i=1}^n \dot{m}_{in,i} Ex_{in,i} + \sum_{j=1}^p Q_{in,j} \left(1 - \frac{T_0}{T_{h,j}}\right) + Q_{leack} \left(1 - \frac{T_0}{T_{air}}\right) + W_{in} - \sum_{k=1}^q \dot{m}_{out,k} Ex_{out,k} - \sum_{L=1}^r Q_{out,L} \left(1 - \frac{T_0}{T_{C,L}}\right) - W_{out} - \Delta E \dot{x}_D =$$

Exergy rate of change Equation 11

Where:

$Ex_{in,i}$ and $Ex_{out,k}$: inlet and outlet-specific exergy

$\Delta E \dot{x}_D$: Destruction rate

$\dot{m}_{in,i}$ and $\dot{m}_{out,k}$: the mass flow of inlet and outlet streams

$Q_{in,j}$ and $T_{h,j}$: condensation rate of steam and temperature

$Q_{out,L}$ and $T_{C,L}$: boiled feed water evaporation rate and temperature

Q_{leack} and T_{air} : heat leak and air temperature

W_{in} and W_{out} : work produced and consumed through shaft or electricity

T_0 : Reference temperature

n, q , p, and r : number of inlet streams, outlet streams, and number of utility heat exchangers for heating and for cooling respectively.

Herein, the exergy flow in the form of mass takes into consideration both the chemical and physical components of exergy according to equation 12:

$$Ex = ex^{Physical} + ex^{Chemical} \quad \text{Equation 12}$$

The physical exergy was obtained from Aspen Hysis stream properties, while the chemical exergy of a material stream x_i was calculated using equation 13 as follows:

$$ex^{Chem} = \dot{n} (\sum x_i \varepsilon_i + RT_o \sum x_i \ln(x_i)) \quad \text{Equation 13}$$

Where x_i is the composition of component i in the considered stream, ε_i is the standard chemical exergy, R is the universal gas constant ($8.314 \frac{J}{k.mol}$), and T_o is Reference state temperature (25 °C).

6.2. Results and Discussion

Referring to Figure 6-9, 6430 MW exergy NG is fed to the liquefaction process and 317 MW (S-134) from the fractionation unit. The whole process requires 0.95 MW exergy in the form of heat, a total of 119.2 MW work, while 1.77 MW is released to the environment using seawater cooling. The process results in the generation of 5421 MW exergy LNG (S-128), 0.31 MW helium (S-125), and 817.3 MW EFG going to the fuel gas compressors, 327.48 MW (S-109) NGL routed to the fractionation. These results imply that the base case process is encountered with a 90.17 MW total loss.

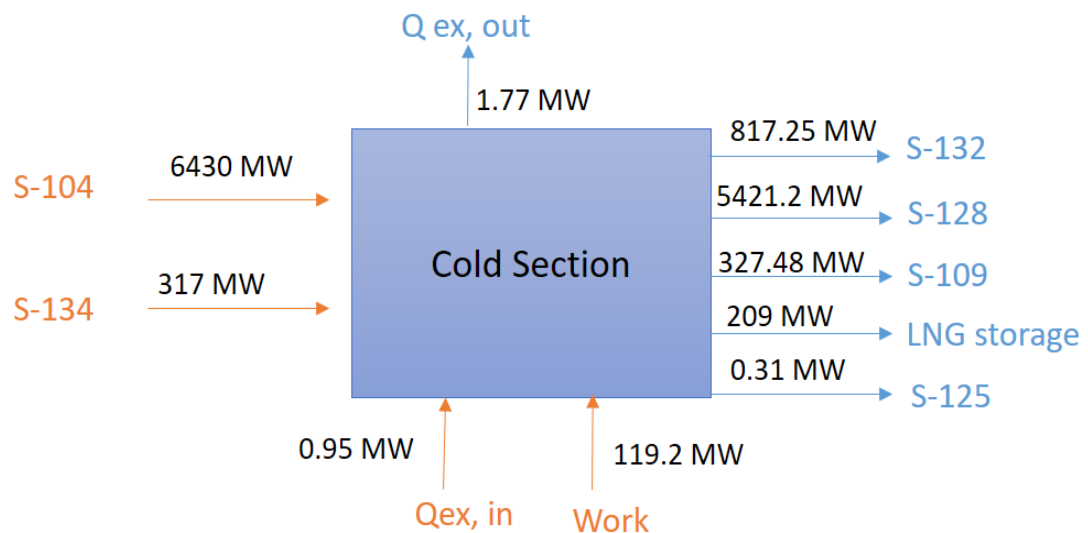


Figure 6-9: Exergy Diagram for the base case

Referring to Figure 6-10, 6718 MW (S -104) and 320 MW LNG (S-134) are fed to the liquefaction unit, respectively. The energy requirement of the process is close to what was seen in the base case scenario, such that an amount of 0.99 MW and 117.9 heat and work are required, respectively. While 1.8 MW is transferred to seawater, generating 6067.48 LNG, 342.08 MW NGL, and 662.07 MW EFG. Thus, destroying nearly 83.63 MW exergy, which is a 7.25% lower loss compared to the base case scenario. This is in line with the previously reported results of the proposed scenario has lower energy consumption and SPC compared to the base case. This might be attributed to the absence of NRU unit equipment and eventually less equipment where exergy loss occurs.

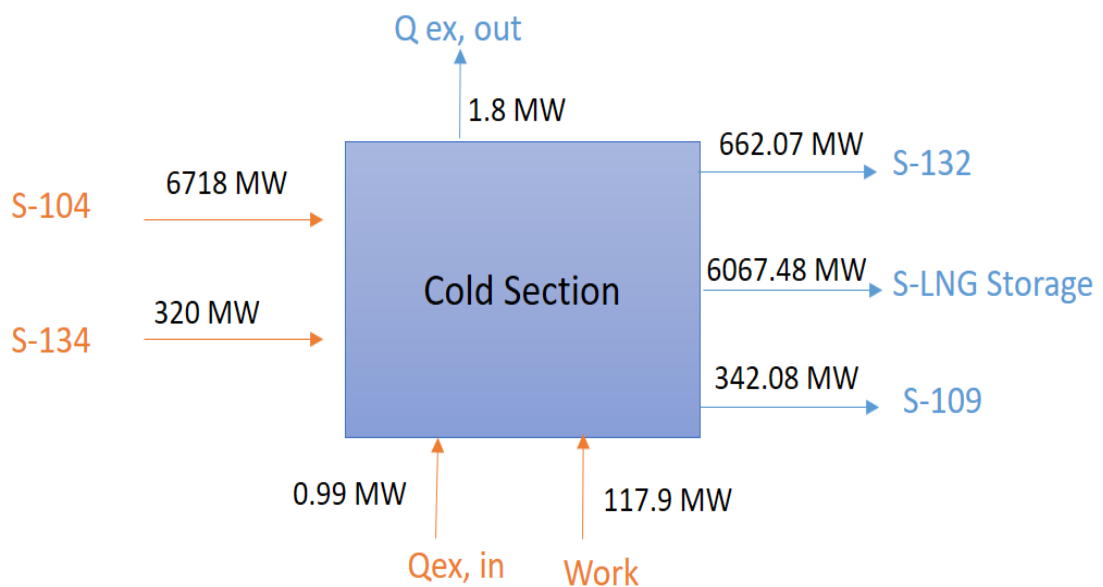


Figure 6-10: Exergy Diagram for 87.5% UNrem

The exergy loss here gives a sense of comparison between the base case and the

proposed case utilizing exergy loss. However, further improvements require identifying the optimization and retrofitting opportunities, which in turn requires highlighting the main contributors to the total exergy loss.

Thus, rigorous and detailed exergy analysis is required to quantify the exergy destruction across equipment (i.e. Compressors, heat exchangers, and columns). This will guide the focus towards components where improvements could be made to enhance the efficiency of the process.

In the same context, the exergy efficiency of the processes was calculated using equation 14:

$$\eta = \frac{\sum Ex_{out}}{\sum Ex_{in}} = 1 - \frac{Ex_D}{\sum Ex_{in}} \quad \text{Equation 14}$$

According to

Table 6-10 which presents the exergy loss and efficiency obtained values, results revealed that the exergy efficiency of the base case and the proposed scenario is 98.6% and 98.83% respectively, which is a 0.23% improvement. The high-efficiency values indicate that improving the processes is limited and not much optimization/retrofitting can be done.

Table 6-10: Exergy Results for the base case and scenario 8

	Base case	87.5% UN_{rem}
Exergy Loss (MW)	90.71	83.63
Exergy Efficiency (%)	98.6%	98.83%

CHAPTER 7: TECHNOLOGIES USED FOR UPFRONT NITROGEN REMOVAL

7.1. Introduction

To verify the effectiveness of the UN_{rem} , an efficient removal technology should be selected in terms of removal efficiency and cost. It is mainly based on the physical removal of nitrogen from adsorbents. Asma et al shortlisted the different chemical and physical possible separation processes. As physical separation, it presents the adsorbent systems with their operating conditions and selectivity. Moreover, it presents the nitrogen separation with membranes and its permselectivity. Hybrid systems of absorption and membranes can be used for a higher nitrogen selectivity process without the need for methane recompression. Distillation can be used by integrating the nitrogen removal process with the NGL recovery column. For chemical separation, several technologies can be used such as chemical absorption, gas hydrates, and lithium-based. Literature shows that physical and chemical separation processes are either expensive or result in low-efficiency separation. [42] Thus, the selection of UN_{rem} can be based on the highest removal efficiency process and compensate for the high cost by the process product sales. By studying the best physical removal of nitrogen by adsorbents, lithium metal has a priority among other conventional adsorbents to remove nitrogen from NG. Rufford et al state from experiments that the theoretical uptake of nitrogen on lithium (24 mmol N_2 / gram lithium) is an order of magnitude higher than the best nitrogen selective adsorbent reported in the literature.[43] Moreover, lithium and methane do not react but it has a high selectivity for nitrogen when the reaction is completed, methane can be fully recovered. Starting from this concept, researchers have focused on investigating the extent of lithium-nitrogen capture reaction at ambient temperature to separate the nitrogen from hydrocarbon streams. Gu et al, Jain et al, Li, McEnaney, et al showed that at ambient temperature lithium does not react with

nitrogen although it reacts with the lithium moisture. [44-46] M. Schiemann et al studied and presented the efficiency of lithium electrowinning from lithium hydroxide by molten salt electrolysis. [47] More investigation on this process was done by Takeda et al where they fed lithium hydroxide into an anode compartment separated from lithium metal deposited at the cathode by a porous magnesia diaphragm and obtained a current efficiency of 84-86%. [48] Also, McEnaney designed a molten electrolysis cell with a porous alumina diffusion barrier around the counter electrode to mitigate the side reactions leading to the consumption of lithium product deposited at the cathode and achieved current efficiency of 88.5%. [46] The experimental results can be applied to the Arrhenius equation to obtain the kinetics of the reaction. Although, up to this time, the accurate kinetic model is not well established.[49] These experiments showed a great improvement in nitrogen capture using lithium, further investigation should be done in order to be developed for a large-scale application.

7.2. Techniques of nitrogen capture from NG

Several methods of UN_{rem} are studied for large-scale applications. It is divided into three main methods physical/chemical separation and gas hydrate. Physical separation of upfront nitrogen from a hydrocarbon stream can be applied through the usage of membranes, gas adsorption, and distillation under cryogenic conditions. The adsorption method was economically advantageous compared to other methods. Its efficiency depends on the selectivity and capacity of the adsorbents used. Table 7- 1 presents the adsorbents' characteristics such as selectivity, cost and materials used that can be applied for nitrogen removal. Obviously, the selectivity varies depending on the components, the PAF and CMS show a significant selectivity for nitrogen over hydrocarbons. The cost of most adsorbents is depending on the material and the manufacturing process, usually organic materials are cheaper than sophisticated ones.

Table 7- 1: Adsorbents characteristics for nitrogen removal

	Material	Cost	Selectivity	Ref
MOFs	Metal ions and organic ligands	low	High	[50, 51]
Zeolites	Microporous aluminosilicates	low	High	[52]
PAFs	Sophisticated natural and artificial zeolites	Depending on the synthetic method	- exceptional for the GHGs - low for other gases	[53]
Activated carbon	Adsorbent (RTL 7–9)	low	low	[54, 55]
CMS	Natural adsorbents: coconut shell and coal	low	High for the nitrogen	[56, 57]
Titanosilicates	natural minerals and synthesized material	Low operational cost	High for the nitrogen	[58, 59]

Another physical separation method is the membranes where pressurized gas passes through the membranes to a lower pressure region. It is an economical and effective method for gas separation.[60] The common type of membrane used for CH₄ and N₂ separation is the MMM which has a better performance and more stable mechanical properties than polymer membranes. It can be customized by increasing the selectivity

for gases to be removed and increasing permeability for the other gases in the stream, eg: N₂/ CH₄, CO₂/N₂ systems, the membrane can be customized to have a higher selectivity for nitrogen in the first system and the carbon dioxide in the second system. [61-63] Table 7- 2 presents the characteristics of membranes used for the methane nitrogen separation. Each membrane has its specific operational conditions for optimal performance. The permselectivity of membranes is the most important evaluation criterion for the system efficiency, it is a measure of membrane ability to separate between anions and cations through the concentration potential between both fluids. [64]

Table 7- 2: Membranes characteristics for methane-nitrogen separation

Membrane type	Operation conditions	Selected Component	Permselectivity	Ref
Fluorinated polyimides	up to 60 bar 65 °C	N ₂	1	[65]
MMM (Amide and CLINO)	10 bar 35 °C	CO ₂ then N ₂	CO ₂ : 31.77 N ₂ : 1.87	[66]
perfluorinated polymers (Hyflon® AD 60)	14 bar 22 °C	CO ₂ then N ₂	2.3 for N ₂	[67]
Zeolite membrane (SSZ-13)	7 bar 25 °C	N ₂	13	[68, 69]

Chemical separation is based on the reactivity of one component compared to another in the same gas stream. As this thesis work focuses on methane-nitrogen separation; several solvent media were studied. Table 7- 3 mentioned the chemical processes for the CH₄ / N₂ separation, all removal processes have a higher selectivity toward the nitrogen compared to the methane in the same gas stream. Different solvents can be used for absorption and adsorption with specified operating conditions. These methods result in a high product purity which validates their effectiveness.

Table 7- 3: Chemical processes for methane-nitrogen removal

Removal method	Solvent	Operating conditions	Selected component	Product purity	Ref
Absorption	TMC Solution	3–30 bar	N ₂	1.7-2.4	[70]
	(K-[RuII(EDTA)])	30 °C		(selectivity)	
	FeII phosphine complexes	Low T and P	N ₂	-	[71]
	Ligands and TMCs	69 bar	N ₂	-	[72]
		20 °C			
		solution			
Adsorption	Organometallic complex solution	69 bar	N ₂	4% N ₂	[73]
		20 °C		96% CH ₄	
	Lithium	8.8 bar	N ₂	2% N ₂	[74]
		60 °C			
	Moisture-pretreated lithium	80 bar	N ₂	<0.5% N ₂	[44]
		25 °C			

To select the optimal method for separation, the process should be fully studied with its operational conditions and nitrogen content in the feed taking into account the purity of the final product of the LNG plant that should stand within the global specifications. Chemical processes take advantage of having a higher selectivity for the separated fluid which results in higher product purity. Hybrid processes can be implemented for an effective separation method, absorption, and membrane system shows a significant

enhancement for the separation effectiveness compared to the membranes only.[75]

To compare the techniques used for the nitrogen capture from hydrocarbons stream, the pugh matrix is used to score the techniques criteria such as energy efficiency, cost, nitrogen selectivity, etc. As shown in table Table 7- 4, compared to the actual process, each criterion is scored as positive (1), negative (-1), or equal (0) depending on how much it is meeting the criteria. Most of the technologies are either methane selective or need high energy for separation. As the capture process should be profitable and does not result in any extra cost, membranes were ranked at the bottom of the list because of the high energy consumption, high cost, and low nitrogen selectivity compared to hydrocarbons. Nitrogen fixation by lithium shows the best alternative in terms of nitrogen selectivity, cost, and operating conditions.

Table 7- 4: Pugh matrix for upfront nitrogen removal different technologies

Technology	Energy efficiency	Cost	N2 selectivity	Operating conditions	Scalability	Total	Rank
Distillation	0	-1	-1	-1	1	-2	4
Adsorption	0	1	-1	0	0	0	3
Membrane	-1	-1	-1	-1	0	-4	7
Bio N2 fixation	-1	1	1	0	1	2	2

Technology	Energy efficiency	Cost	N2 selectivity	Operating conditions	Scalability	Total	Rank
Electrochem N2 fixation	0	-1	1	-1	-1	-2	4
N2 fixation by Haber-bosh	-1	0	0	-1	0	-2	4
N2 fixation by lithium	0	1	1	1	0	3	1

Moreover, since nitrogen and lithium can react directly at ambient temperatures where lithium does not react with methane in case of a mixture; it gives this capture technique the advantage over others. This reaction should be at a temperature of the lower melting point of lithium for safety reasons. To be applied within the LNG supply chain profitably; lithium should be regenerated because of its high price and high consumption to capture the large amounts of nitrogen. Thus, a loop of lithium recycling can be applied to ensure the continuous supply of lithium. It is composed of three steps: nitridation, hydrolysis, and electrolysis. First, the lithium is processed through a direct nitridation by nitrogen, pure methane stream is produced. (Reaction 1) The nitrogen-lithium reaction produces lithium nitrate that is being hydrolyzed to produce ammonia as a valuable product and lithium oxide. (Reaction 2) In the second stage, lithium oxide is added to hydrochloric acid to be converted to lithium chloride. (Reaction 3)

For lithium regeneration, electrolysis of lithium chloride converts it to lithium metal that is recycled to nitrogen capture again. In addition, The chlorine by-product can be also recycled to form the hydrochloric acid used in the second step. (Reaction 4)

The following reactions show the complete cycle of lithium regeneration and ammonia, hydrochloric by-product formation. [74]



This

Work

Hajer:
Ajinkya:

CHAPTER

8.1.

To

Table

Class	Purpose	Level	Cost (%)
Class	Screening	0	±
Class	Preliminary	1	±
Class	Definitive	10	±
Class	Detailed	30	±

After

8.2.

The cost estimation for the process requires basic relationships between cost and design to have a rough expenditure assessment to start the project or to enhance the process. CAPEX and OPEX analyses are conducted for the seven cases of UN_{rem} to check the feasibility of each case and the profit accompanied by the removal. Similarly, for the lithium cycle which is selected as the removal technology; in this way, the profit of these technologies can be calculated. As the rigorous design information for equipment is achieved in an earlier stage of this thesis; it is sufficient data to conduct a class 4 and class 5 cost estimation. All data on equipment designs, pressure, power, and heat load are taken from the HYSYS™ simulation results. First, the CAPEX analysis was based on calculating the equipment cost in the cold section such as pumps, compressors, MSHE, etc. $CBM = C_p F_{BM}$

$$C_{BM} = C_p F_{BM} \quad \text{Equation 15}$$

Where: C_{BM} = cost bare module (direct and indirect cost)

C_p = cost of the purchase in base conditions

F_{BM} = multiplication factor for the material of construction and operating pressure

$$\log(C_p) = K_1 + K_2 \times \log(A) + K_3 \times [\log(A)]^2 \quad \text{Equation 16}$$

Where K_1, K_2, K_3 = correlation constants specific for each equipment (Table 8-12)

A= size of equipment

Table 8-12: Correlation constants for equipment

Equipment	K₁	K₂	K₃
Centrifugal	3.3892	0.0536	0.1538
Centrifugal	2.2897	1.3604	-
Columns	3.4974	0.4485	0.1074
Kettle	4.4646	-	0.3955
Water	4.1884	-	0.1974
MSHE	4.6656	-	0.1547

Results found for the bare module cost are estimated at 2001, it has to be converted to the present time by applying the Chemical Engineering Plant Cost Index (CEPCI)

$$CBM_{2020} = C_{2001} \left(\frac{I_{2020}}{I_{2001}} \right)$$

Equation 17.

$$C_{BM2020} = C_{2001} \left(\frac{I_{2020}}{I_{2001}} \right) \quad \text{Equation 17}$$

Where C_{BM2020} = total equipment cost in 2020

I_{2020} = the cost index of the present year

I_{2001} = the cost index of the year 2001

Calculations of columns' cost are different from the other equipment as it has to include the cost of the tray with the tower cost. Tray cost is dependent on the number of trays, type, and operating pressure whereas the tower cost is dependent on the volume and

pressure. For the tower cost, C_p is calculated using Equation 16 then the multiplication factor using Equation 18, Equation 19, and Equation 20.

$$F_{BM} = 2.25 + 1.82 \times F_M \times F_P \quad \text{Equation 18}$$

Where F_M = constant for stainless steel towers

F_P = pressure factor

$$F_{p,vessel} = \frac{\left(\frac{PD}{(2)(944)(0.9)-1.2P}\right)+CA}{t_{min}} \quad \text{Equation 19}$$

where D= diameter (m)

P = pressure t operation in barg

CA = corrosion allowance

T_{min} = minimum vessel thickness

$$C_{BM,tower} = F_{BM} \times C_p \quad \text{Equation 20}$$

The total cost of the trays is calculated using Equation 21, the bare module cost of trays and vessels is added up to get the total cost of the columns for all UN_{rem} scenarios.

$$C_{BM,trays} = C_p \times N \times F_{BM} \times F_q \quad \text{Equation 21}$$

Where N= number of trays

F_q = quantity factor for trays

Second, the OPEX analysis is based on calculating the direct expenses such as utilities used in the cold section which are the cooling water and steam, and the labor cost. Also, the fixed costs such as taxes and depreciation. Values of utilities' flow rates are extracted from the HYSYS™ simulation and multiplied by its price in US dollars. The labor cost is estimated depending on the average salary of workers in Qatar LNG plants. Table 8-13 presents all relationships used for the OPEX estimate, the summation of these numbers results the OPEX for 1 year. As the plant lifetime is estimated to be 20 years, the results are multiplied by 20.

Table 8-13: Relations used for the OPEX estimate

	Supervision	0.18 x operating labor cost
Direct Manufacturing Costs (DMC)	Maintenance	0.06 x CAPEX
	Operating supplies	0.009 x CAPEX
	Lab charges	0.15 x operating labor
	Depreciation	0.05 x CAPEX
Fixed Manufacturing Costs	Taxes & Insurance	0.032 x CAPEX
	Overhead Cost	(0.708 x Operating labor)+(0.036x CAPEX)
	Admin	(0.177 x Operating labor)+(0.009 x CAPEX)
General Expenses	Distribution	0.11 x DMC
	R&D	0.005 x DMC

It is important to evaluate the cost of the UN_{rem} technology to check the economic feasibility of the full process. In which, the lithium cycle profitability is evaluated in terms of raw material cost and revenue from the ammonia produced. To evaluate the capital cost of the lithium cycle, the cost of the lithium reactor, hydrolyzer, and electrolyzer are calculated using the same methodology cited above. The size of each unit is based on the capacity and the amount of nitrogen removed through the stoichiometry of the reactions presented in chapter 7. All values of reactants and products' molar flow for the nitrogen fixation by the lithium process are presented in Table 8-14.

Table 8-14: Molar flows of inlet and outlet streams in removal technology

	UN_{rem} (kmol/h)	Li Required (kmol/h)	Water for Li₃N hydrolysis (kmol/h)	NH₃ Produced (kmol/h)
Base Case	0	0	0	0
Scenario - 1	154	922	922	307
Scenario - 2	309	1855	1855	618
Scenario -3	467	2800	2800	933
Scenario - 4	610	3660	3660	1220
Scenario -5	788	4726	4726	1575
Scenario - 6	951	5707	5707	1902
Scenario - 7	1117	6701	6701	2234

The price of ammonia is based on the US sale price.[79] The electricity used in the regeneration step of lithium should be taken into account. Table 8-15 presents the parameters used for the capital cost estimation of nitrogen-lithium capture such as the cost of the raw materials and electricity needed for the system.

Calculating the overall capital cost of UN_{rem} and the lithium cycle can prove the economic profitability of the full process compared to the base case.

Table 8-15: Parameters used for the lithium cycle capital cost estimation

Design Specification	Value	Reference
Number of lithium reactors	3	[74]

Lithium Cost, \$/Tonne	110000	[80]
Ammonia Price, \$/Tonne	400	[79]
Electricity cost (E_{cost}), \$/kWh	0.033	[81]
Electrolysis temperature, °C	400	[74]

8.3. Results and discussion

Following the methodology presented earlier for the cold section with the removal technique, the results are shown to demonstrate the profitability of the upfront nitrogen removal that based upon it; this technique is verified.

Figure 8-11 presents the trend of CAPEX and OPEX for the cold section in the seven UN_{rem} cases. Results show the decrease of costs as the upfront nitrogen is removed, it declines from 12.51 Billion US dollars in the base case to 11.11 Billion US dollars in the case of 82.5% UN_{rem} which is a significant decrease for a 20 years plant lifetime. The important reduction starts at a removal percentage of 37.5 % with a cost of 11.72 billion US dollars with a decrease of 4.63% from the 25% UN_{rem} scenario.

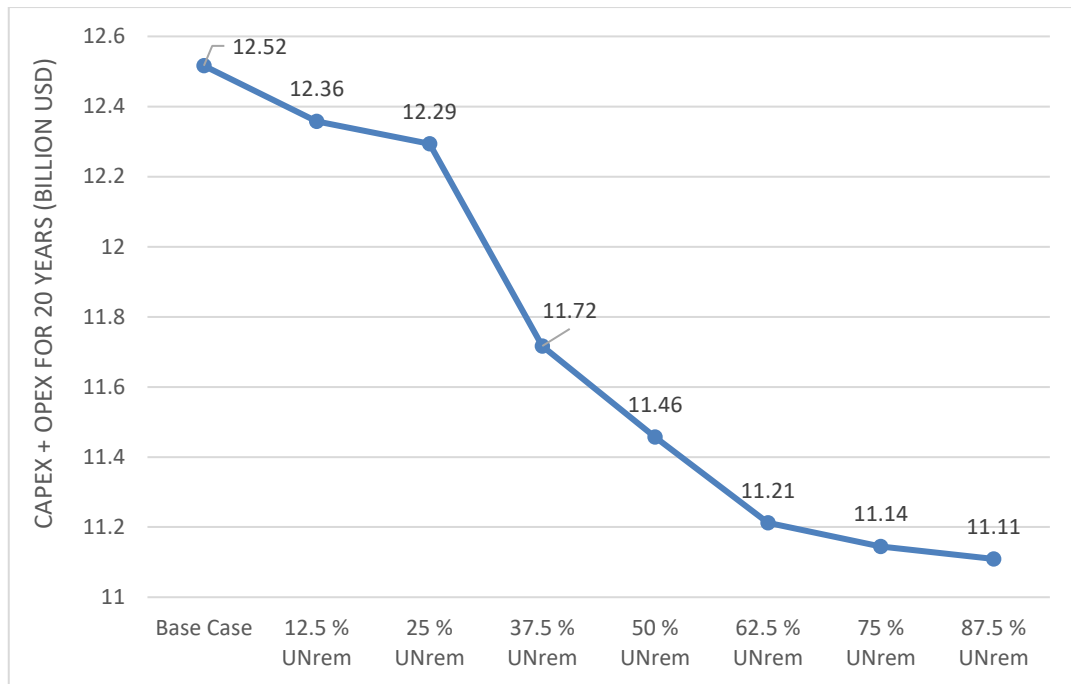


Figure 8-11: The overall CAPEX and OPEX for the cold section in all UN_{rem} scenarios

For a detailed analysis, Figure 8- 12 shows the share of each piece of equipment in CAPEX for the best removal scenario 7. It can be noticed that the compressors and MSHE have the highest share in the total CAPEX with 59% and 34% respectively. These major contributions are conducting the main fluid transformation, thus bigger sizes and better performance should be selected. The water coolers have a share of 7%. Whereas, the pumps and columns have the lowest share with 0.004% and 0.003% respectively this can be explained by the low number and moderate size of pumps and columns available in the process compared to compressors and MSHE.

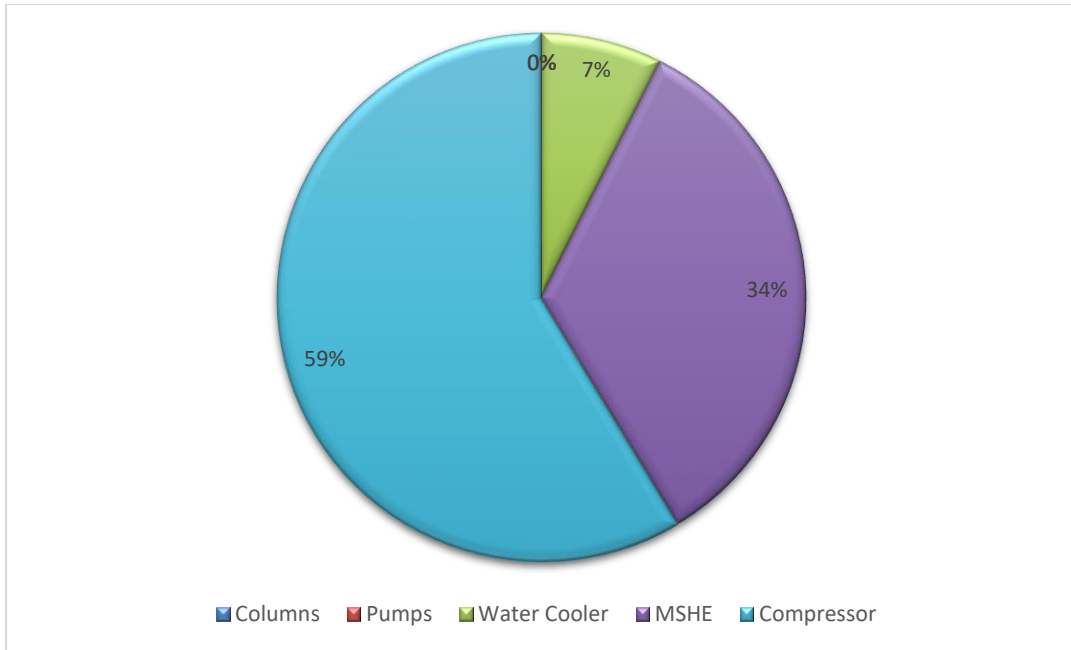


Figure 8- 12: Distribution of CAPEX cost in scenario 7 among the process equipment

Figure 8-12 presents the percentage share of the OPEX parameters in scenario 7, the fixed manufacturing costs including the taxes, depreciation, and overhead cost have the highest share of 48%. The direct manufacturing cost that consists of utility, labor, maintenance, etc.. has a 32% of the total OPEX. The least share was assigned to the general manufacturing cost with 20% such as the admin, research, and development which are always variable depending on the budget and resources.

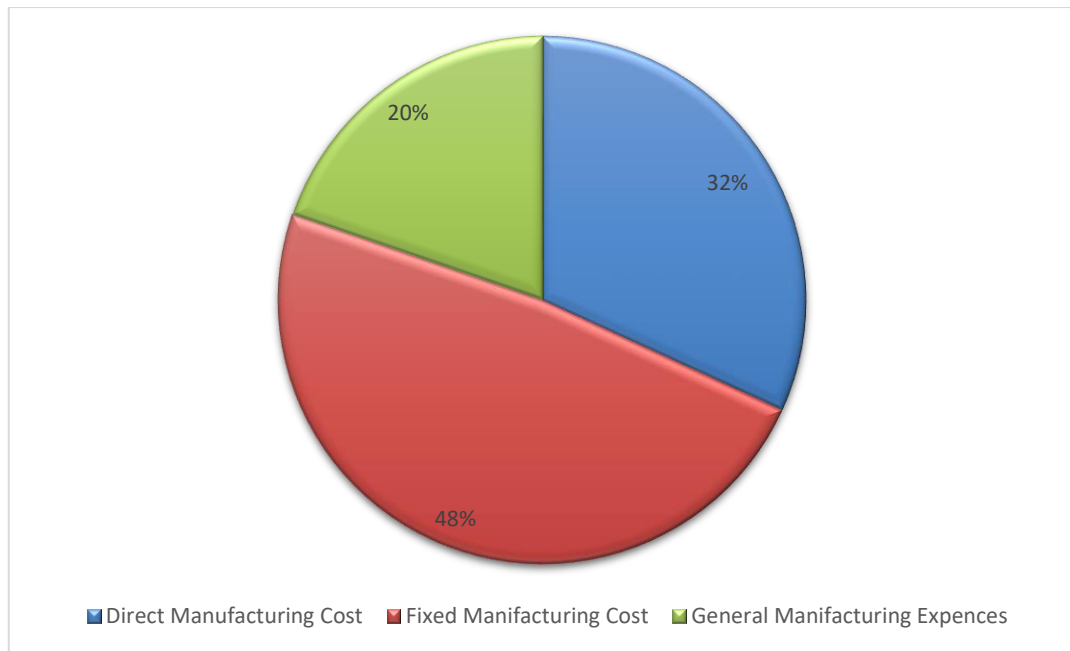


Figure 8-12: Share of OPEX parameters in scenario-7

As found in an earlier stage of this thesis, the removal of upfront nitrogen can increase the LNG production rate. Figure 8-13 shows the revenues of selling the extra LNG produced from the seven UN_{rem} scenarios. In the case of 12.5%, UN_{rem} revenues increased to 34.48 billion US dollars which have increased by 0.5 % compared to the base case. Revenue keeps increasing for all scenarios where it can reach 35.92 billion US dollars in the case of 87.5%. This can show a difference of 4.54 % compared to the base case. An important increase in revenue sales over the 20 years can validate the idea of UN_{rem} economically.

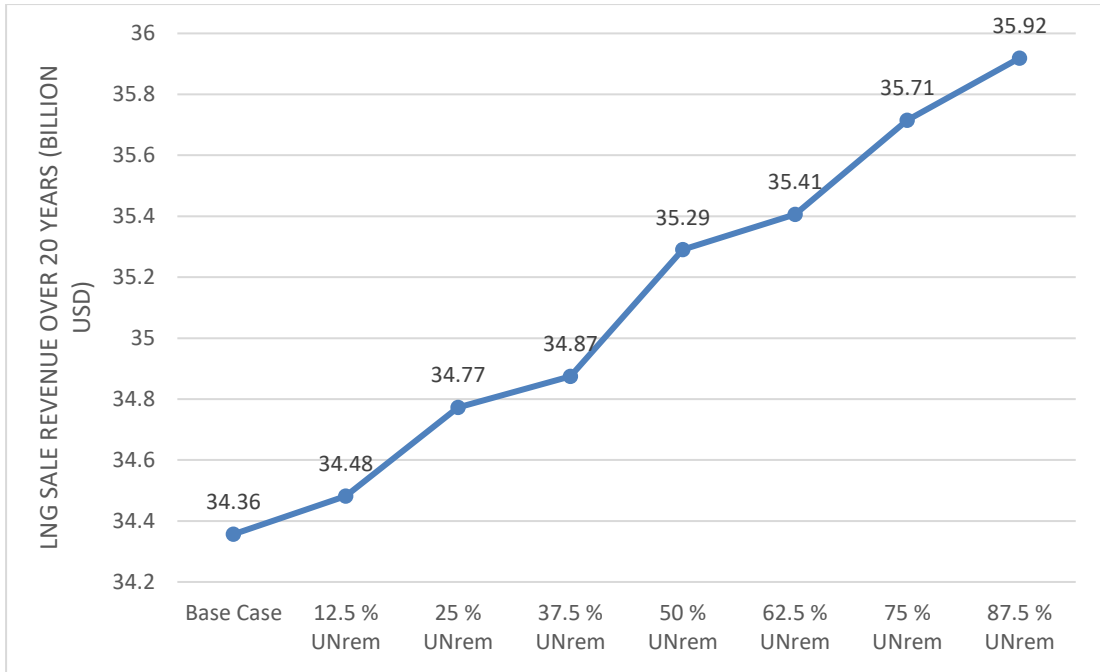


Figure 8-13: LNG sale revenue over 20 years for the UN_{rem} scenarios

The lithium cycle removes the nitrogen from the hydrocarbon stream and produces ammonia that can be commercialized. Figure 8-14 presents the capital cost and manufacturing cost for the lithium cycle technology in all UN_{rem} scenarios. The overall trend is increasing from 0.57 billion USD in the 12.5% UN_{rem} case to 3.33 billion USD in the case of 87.5% UN_{rem}. It is an expected trend as removing higher nitrogen fractions in the hydrocarbon stream will need higher electricity usage and raw material. For the other removal cases, the CAPEX and OPEX results 0.96, 1.46, 1.94, 2.52 and 2.79 USD for 25%, 37.5%, 50% ,62.5% and 75% UN_{rem}. The increase is not significant and is recovered by ammonia sales in the later stages of the lithium cycle.

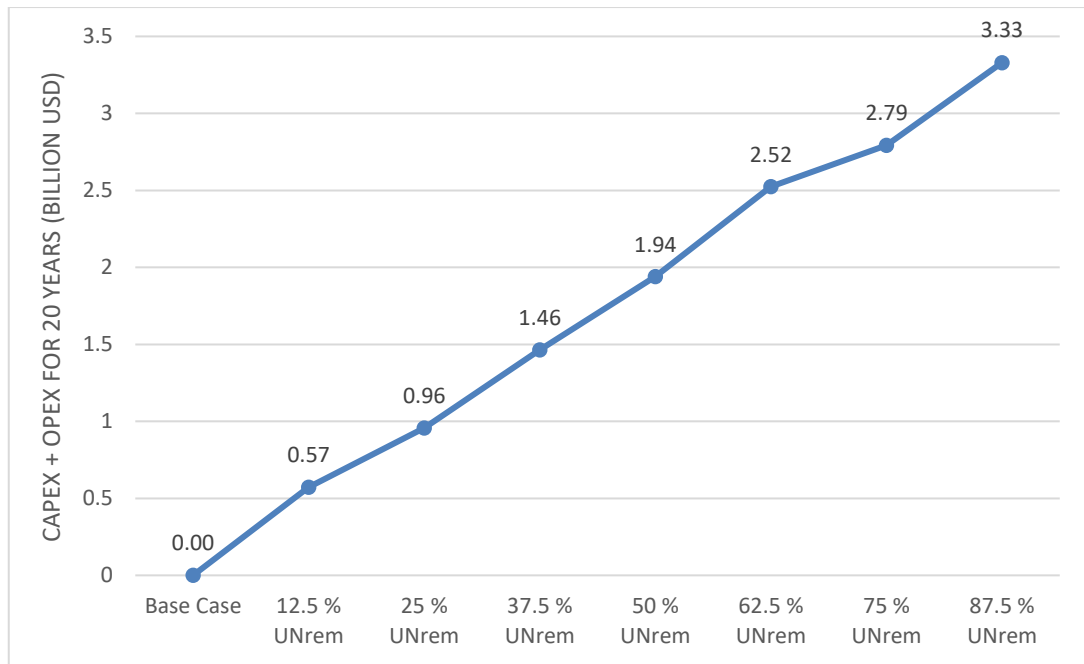


Figure 8-14: CAPEX and OPEX of removal technique for UN_{rem} scenarios

Figure 8-15 presents the ammonia sales from each removal case, it shows a significant increase as the nitrogen is removed. The ammonia revenue is estimated to be 0.73 billion USD in the case of 12.5% UN_{rem} increased to 0.74 USD in the case of 25% UN_{rem}. For the cases, 37.5%, 50%, 62.5%, and 75% of the sales are 1.11, 1.45, 1.88 and 2.27 billion USD, respectively. The revenues can reach up to 2.66 billion USD in the case of 87.5% UN_{rem}. The lithium cycle is proven as an effective technology for UN_{rem} where it decreases the nitrogen fraction in the hydrocarbon stream from 10% to 0.5%.

[42]

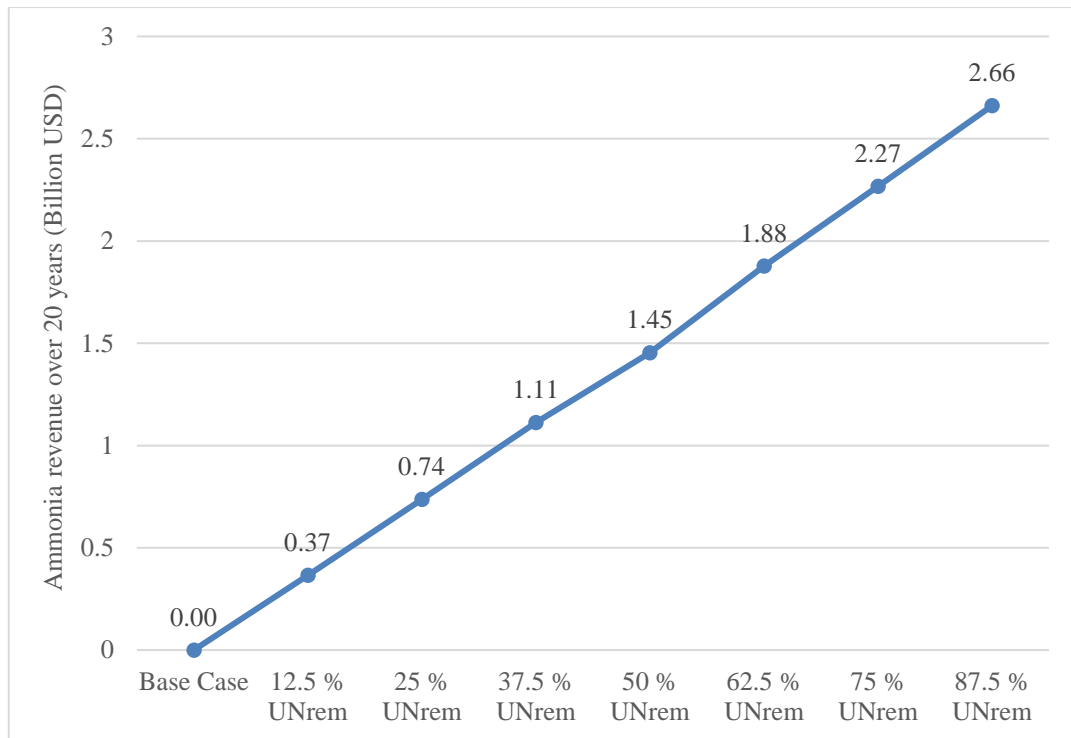


Figure 8-15: Ammonia sales for the UN_{rem} scenarios

After the economic analysis of the UN_{rem} technique and the lithium cycle, the total profit made from both techniques is calculated to check if the total expenses can be recovered by the total profit from the LNG and ammonia sales.

Table 8-16: Profit of UN_{rem} technology with the lithium cycle for 20 years

UN _{rem} Cases	Total revenues – Total expenses (Billion USD)
12.5 % UN _{rem}	21.9
25 % UN _{rem}	22.2
37.5 % UN _{rem}	22.8
50 % UN _{rem}	23.3
62.5 % UN _{rem}	23.5

UN_{rem} Cases	Total revenues – Total expenses (Billion USD)
75 % UN_{rem}	24
87.5 % UN_{rem}	24.1

Table 8-16 presents the profit for 20 years from the LNG product sales in the cold section and the ammonia sales in the lithium cycle, results show that the profit resulting from 12.5% UN_{rem} is 21.9 Billion USD. As the nitrogen fraction removed is increasing, the total profit of the process increases to 22.2, 22.8, 23.3, 23.5, 24 and 24.1 billion USD for the cases of 25%, 37.5 %, 50%, 62.5%, 75% and 87.5%, respectively. As mentioned in previous chapters of the thesis, increasing the nitrogen removal fraction increases the LNG product thus it increases its sales and more ammonia is also produced. In this, it is validated through the results found. The lithium cycle accompanied by the UN_{rem} technique is an economically profitable method for removing nitrogen, decreasing power requirements with increasing the process productivity.

CONCLUSIONS AND RECOMMENDATIONS

Energy optimization is important in the LNG industry, especially with the increasing demand in the LNG market. With the current global NG market, It is challenging to increase production without an increase in power consumed and an increase in plant expenses. For this reason, technical enhancements to the current plant should be applied.

This thesis work studies the optimization of refrigerant components with UN_{rem} for an energy-economy efficient plant. The focus was on the intensive-energy stage within the LNG chain which is liquefaction. Seven different removal scenarios are studied using HYSYS™ and Matlab™ software integrated for optimization. The aim is to decrease the total energy consumed in the C_3MR cycle by studying the effect of refrigerant flow rates and their heat capacity. For robust and realistic results, the plant was simulated rigorously using HYSYS™ which mimics an actual LNG cold section with its operational conditions. This step is valuable to obtain a more realistic and adjustable simulation depending on the objective of the thesis. The results of the optimization of MR composition on UN_{rem} cases show that in the case of 87.5% UN_{rem} , an increase of LNG product flow rates by 4.4 %, 0.241% decrease in total energy consumption of the process, and a decrease of 4% for SPC compared with the base case. This effect was similar for all removal percentages. The exergy analysis of the best upfront nitrogen removal scenario (87.5%) reveals a decrease in exergy loss by 7.08 MW and an increase in exergy efficiency by 0.23% compared to the base case. It is necessary to select the best nitrogen removal method that satisfies the best nitrogen selectivity, energy efficiency, and cost. Several methods are available in the literature as membranes, chemical reactions, etc, As a result, nitrogen fixation by lithium was selected for its potential in separating nitrogen from hydrocarbons at ambient temperature.

The last step is to verify the profitability of the UN_{rem} for all scenarios. The capital cost and operational cost are calculated based on the optimization results taking into account the nitrogen fixation by lithium as a removal technology. This method can result in a profit of 24.1 Billion USD in the case of 87.5% UN_{rem} for a 20 years plant which makes this methodology profitable and economic.

In conclusion, with the removal of upfront nitrogen; the plant can produce higher flows of LNG product with the same energy consumed and the same high product quality. This can affect the rate of products from the removal technique which can be also commercialized. These results can be enhanced using other boundaries that can broaden the search space and gives more accurate results. In addition, other removal techniques can be studied and economically analyzed for a profitable process. The feasibility of the 100% UN_{rem} case can be further studied with the investigation of the possible removal processes that fit within the process.

REFERENCES

1. Bataille, C., et al., *A review of technology and policy deep decarbonization pathway options for making energy-intensive industry production consistent with the Paris Agreement*. Journal of Cleaner Production, 2018. **187**: p. 960-973.
2. Zhang, J., et al., *Comprehensive review of current natural gas liquefaction processes on technical and economic performance*. Applied Thermal Engineering, 2020. **166**: p. 114736.
3. Lu, Y., et al., *China's black carbon emission from fossil fuel consumption in 2015, 2020, and 2030*. Atmospheric Environment, 2019. **212**: p. 201-207.
4. Le Fevre, C.N., *A review of demand prospects for LNG as a marine fuel*. 2018.
5. Pfoser, S., O. Schauer, and Y. Costa, *Acceptance of LNG as an alternative fuel: Determinants and policy implications*. Energy Policy, 2018. **120**: p. 259-267.
6. He, T., et al., *LNG cold energy utilization: Prospects and challenges*. Energy, 2019. **170**: p. 557-568.
7. Katebah, M.A., et al., *Rigorous simulation, energy and environmental analysis of an actual baseload LNG supply chain*. Computers & Chemical Engineering, 2020. **141**: p. 106993.
8. Łaciak, M., et al., *Possibilities of Liquefied Natural Gas (LNG) use for power generation*. IOP Conference Series: Earth and Environmental Science, 2019. **214**: p. 012138.
9. Pal, A., E.I. Al-musleh, and I.A. Karimi, *Reducing Power Use in the Cold Section of LNG Plants*. ACS Sustainable Chemistry & Engineering, 2021. **9**(38): p. 13056-13067.

10. Lee, Y., Y. Lim, and W.B. Lee, *Integrated Process Design and Optimization of Nitrogen Recovery in Natural Gas Processing*. Industrial & Engineering Chemistry Research, 2019. **58**(4): p. 1658-1674.
11. Ghorbani, B., et al., *Cascade refrigeration systems in integrated cryogenic natural gas process (natural gas liquids (NGL), liquefied natural gas (LNG) and nitrogen rejection unit (NRU))*. Energy, 2016. **115**: p. 88-106.
12. Eterafi, S., S. Gorjian, and M. Amidpour, *Thermodynamic design and parametric performance assessment of a novel cogeneration solar organic Rankine cycle system with stable output*. Energy Conversion and Management, 2021. **243**: p. 114333.
13. Chen, F., M. Okasinski, and T. Sabram, *Novel Nitrogen removal schemes for LNG plants with electric motor drive and varying feed composition*. LNG18,(Perth, Australia), 2016.
14. Pal, A., E.I. Al-musleh, and I.A. Karimi, *Development and optimization of an energy efficient and self-sustained integrated process for nitrogen removal for baseload LNG plant*, in *Computer Aided Chemical Engineering*, M. Türkay and R. Gani, Editors. 2021, Elsevier. p. 1671-1676.
15. Montanez-Morantes, M., M. Jobson, and N. Zhang, *Operational optimisation of centrifugal compressors in multilevel refrigeration cycles*. Computers & Chemical Engineering, 2016. **85**: p. 188-201.
16. Khan, M.S., et al., *Knowledge based decision making method for the selection of mixed refrigerant systems for energy efficient LNG processes*. Applied Energy, 2013. **111**: p. 1018-1031.
17. Pham, T.N., et al., *Enhancement of single mixed refrigerant natural gas liquefaction process through process knowledge inspired optimization and*

- modification*. Applied Thermal Engineering, 2017. **110**: p. 1230-1239.
18. Nawaz, A., et al., *Optimization of mixed fluid cascade LNG process using a multivariate Coggins step-up approach: Overall compression power reduction and exergy loss analysis*. International Journal of Refrigeration, 2019. **104**: p. 189-200.
 19. Pham, T.N., et al., *Optimization of modified single mixed refrigerant process of natural gas liquefaction using multivariate Coggin's algorithm combined with process knowledge*. Journal of Natural Gas Science and Engineering, 2016. **33**: p. 731-741.
 20. Ghorbani, B., et al., *Structural, operational and economic optimization of cryogenic natural gas plant using NSGAI two-objective genetic algorithm*. Energy, 2018. **159**: p. 410-428.
 21. Ali, W., et al., *Surrogate-assisted modeling and optimization of a natural-gas liquefaction plant*. Computers & Chemical Engineering, 2018. **118**: p. 132-142.
 22. Sabbagh, O., M.A. Fanaei, and A. Arjomand, *Optimal design of a novel NGL/LNG integrated scheme: economic and exergetic evaluation*. Journal of Thermal Analysis and Calorimetry, 2021. **145**(3): p. 851-866.
 23. Taleshbahrami, H. and H. Saffari, *Optimization of the C3MR cycle with genetic algorithm*. Transactions of the Canadian Society for Mechanical Engineering, 2010. **34**(3-4): p. 433-448.
 24. Primabudi, E., T. Morosuk, and G. Tsatsaronis, *Multi-objective optimization of propane pre-cooled mixed refrigerant (C3MR) LNG process*. Energy, 2019. **185**: p. 492-504.
 25. Wu, J. and Y. Ju, *Design and optimization of natural gas liquefaction process using brazed plate heat exchangers based on the modified single mixed*

- refrigerant process*. Energy, 2019. **186**: p. 115819.
26. Qyyum, M.A., N.V.D. Long, and M. Lee, *Design optimization of single mixed refrigerant LNG process using a hybrid modified coordinate descent algorithm*. Cryogenics, 2018. **89**: p. 131-140.
 27. Austbø, B. and T. Gundersen, *Using thermodynamic insight in the optimization of LNG processes*, in *Computer aided chemical engineering*. 2014, Elsevier. p. 1273-1278.
 28. Ghorbani, B., et al., *Exergoeconomic analysis and multi-objective Pareto optimization of the C3MR liquefaction process*. Sustainable Energy Technologies and Assessments, 2016. **17**: p. 56-67.
 29. He, T., et al., *Impact of mixed refrigerant selection on energy and exergy performance of natural gas liquefaction processes*. Energy, 2020. **199**: p. 117378.
 30. Wang, X., et al., *Propane and iso-butane pre-cooled mixed refrigerant liquefaction process for small-scale skid-mounted natural gas liquefaction*. Applied Energy, 2020. **275**: p. 115333.
 31. Sanavandi, H. and M. Ziabasharhagh, *Design and comprehensive optimization of C3MR liquefaction natural gas cycle by considering operational constraints*. Journal of Natural Gas Science and Engineering, 2016. **29**: p. 176-187.
 32. Hajji, A., M. Chahartaghi, and M. Kahani, *Thermodynamic analysis of natural gas liquefaction process with propane pre-cooled mixed refrigerant process (C3MR)*. Cryogenics, 2019. **103**: p. 102978.
 33. Won, W. and K.S. Lee, *An energy-efficient operation system for a natural gas liquefaction process: Development and application to a 100 ton-per-day plant*. Computers & Chemical Engineering, 2017. **97**: p. 208-219.

34. Wang, M., R. Khalilpour, and A. Abbas, *Operation optimization of propane precooled mixed refrigerant processes*. Journal of Natural Gas Science and Engineering, 2013. **15**: p. 93-105.
35. Husnil, Y.A., et al., *Steady-state optimality analysis for investigating the energy optimal operation of representative natural gas liquefaction cycles*. Energy Procedia, 2014. **61**: p. 552-555.
36. Webb, R.L., *Performance evaluation criteria for use of enhanced heat transfer surfaces in heat exchanger design*. International Journal of Heat and Mass Transfer, 1981. **24**(4): p. 715-726.
37. Ma'arof, M., et al., *Influence of fins designs, geometries and conditions on the performance of a plate-fin heat exchanger-experimental perspective*. Journal of Mechanical Engineering and Sciences, 2019. **13**: p. 4368-4379.
38. Bouabidi, Z., et al., *Towards improved and multi-scale liquefied natural gas supply chains: Thermodynamic analysis*. Computers & Chemical Engineering, 2021. **151**: p. 107359.
39. Prajapati, Y.K., *Influence of fin height on heat transfer and fluid flow characteristics of rectangular microchannel heat sink*. International Journal of Heat and Mass Transfer, 2019. **137**: p. 1041-1052.
40. El Gmili, N., et al., *Particle swarm optimization based proportional-derivative parameters for unmanned tilt-rotor flight control and trajectory tracking*. Automatika, 2020. **61**(2): p. 189-206.
41. Kaniathara, N., et al., *Optimising monthly tilt angles of solar panels using particle swarm optimisation algorithm*. Indonesian Journal of Electrical Engineering and Computer Science, 2021. **23**: p. 75.
42. Almomani, F., et al., *Prospective of Upfront Nitrogen (N₂) Removal in LNG*

- Plants: Technical Communication*. Energies, 2021. **14**(12): p. 3616.
43. Rufford, T., et al., *The removal of CO₂ and N₂ from natural gas: A review of conventional and emerging process technologies*. Journal of Petroleum Science and Engineering, 2012. s **94–95**: p. 123–154.
 44. Gu, Q., et al., *Theoretical Study of Moisture-Pretreated Lithium as Potential Material for Natural Gas Upgrading*. Industrial & Engineering Chemistry Research, 2018. **57**(45): p. 15512-15521.
 45. Jain, A., et al., *A new synthesis route of ammonia production through hydrolysis of metal – Nitrides*. International Journal of Hydrogen Energy, 2017. **42**(39): p. 24897-24903.
 46. McEnaney, J.M., et al., *Ammonia synthesis from N₂ and H₂O using a lithium cycling electrification strategy at atmospheric pressure*. Energy & Environmental Science, 2017. **10**(7): p. 1621-1630.
 47. Schiemann, M., et al., *Combustion of Lithium Particles in N₂—Reaction Rates*. Combustion Science and Technology, 2017. **189**(1): p. 169-186.
 48. Takeda, O., et al., *Electrowinning of lithium from LiOH in molten chloride*. Journal of The Electrochemical Society, 2014. **161**(14): p. D820.
 49. Michèle, P., F. Loic, and S. Michel, *From the drawbacks of the Arrhenius- $f(\alpha)$ rate equation towards a more general formalism and new models for the kinetic analysis of solid–gas reactions*. Thermochemica Acta, 2011. **525**(1-2): p. 93-102.
 50. Wu, Y., et al., *Decorated traditional zeolites with subunits of metal–organic frameworks for CH₄/N₂ separation*. Angewandte Chemie International Edition, 2019. **58**(30): p. 10241-10244.
 51. Kim, T.-H., et al., *Improved methane/nitrogen separation properties of*

- zirconium-based metal–organic framework by incorporating highly polarizable bromine atoms*. *Chemical Engineering Journal*, 2020. **399**: p. 125717.
52. Silva, J.A., et al., *Adsorption equilibrium and dynamics of fixed bed adsorption of CH₄/N₂ in binderless beads of 5A zeolite*. *Industrial & Engineering Chemistry Research*, 2015. **54**(24): p. 6390-6399.
53. Ben, T. and S. Qiu, *Porous aromatic frameworks: Synthesis, structure and functions*. *CrystEngComm*, 2013. **15**(1): p. 17-26.
54. Su, W., et al., *Adsorption properties of N₂, CH₄, and CO₂ on sulfur-doped microporous carbons*. *Journal of Chemical & Engineering Data*, 2018. **63**(8): p. 2914-2920.
55. Liu, F., et al., *Facile preparation of N and O-rich porous carbon from palm sheath for highly selective separation of CO₂/CH₄/N₂ gas-mixture*. *Chemical Engineering Journal*, 2020. **399**: p. 125812.
56. Ghazi-MirSaeed, M. and S. Matavos-Aramyan, *Gaseous Mixtures Separation via Chemically-Activated Nano Silica-Modified Carbon Molecular Sieves*. *Silicon*, 2021. **13**(5): p. 1331-1345.
57. Effendy, S., C. Xu, and S. Farooq, *Optimization of a pressure swing adsorption process for nitrogen rejection from natural gas*. *Industrial & Engineering Chemistry Research*, 2017. **56**(18): p. 5417-5431.
58. Mitariten, M. *Nitrogen removal from natural gas with the molecular gate adsorption process*. in *88th Annual Convention of the Gas Processors Association*. 2009.
59. Salehi, R.N., F. Rahimpour, and S. Sharifnia, *Adsorption of carbon dioxide, nitrogen and methane on modified titanosilicate type molecular sieves*. *Journal of Natural Gas Science and Engineering*, 2017. **46**: p. 730-737.

60. Bernardo, P., E. Drioli, and G. Golemme, *Membrane gas separation: a review/state of the art*. *Industrial & engineering chemistry research*, 2009. **48**(10): p. 4638-4663.
61. Miricioiu, M.G., et al., *Coal fly ash derived silica nanomaterial for MMMs—application in CO₂/CH₄ separation*. *Membranes*, 2021. **11**(2): p. 78.
62. Dong, G., et al., *Enhanced CO₂/N₂ separation by porous reduced graphene oxide/Pebax mixed matrix membranes*. *Journal of Membrane Science*, 2016. **520**: p. 860-868.
63. Zhao, S., et al., *Mixed-matrix membranes for CO₂/N₂ separation comprising a poly (vinylamine) matrix and metal–organic frameworks*. *Industrial & Engineering Chemistry Research*, 2015. **54**(18): p. 5139-5148.
64. Ji, Y. and G.M. Geise, *The role of experimental factors in membrane permselectivity measurements*. *Industrial & Engineering Chemistry Research*, 2017. **56**(26): p. 7559-7566.
65. Tanis, I., et al., *A comparison of pure and mixed-gas permeation of nitrogen and methane in 6FDA-based polyimides as studied by molecular dynamics simulations*. *Computational Materials Science*, 2018. **141**: p. 243-253.
66. Luna, A.d.J.M., et al., *Na⁺/Ca²⁺ aqueous ion exchange in natural clinoptilolite zeolite for polymer-zeolite composite membranes production and their CH₄/CO₂/N₂ separation performance*. *Journal of Natural Gas Science and Engineering*, 2018. **54**: p. 47-53.
67. Lokhandwala, K.A., et al., *Membrane separation of nitrogen from natural gas: A case study from membrane synthesis to commercial deployment*. *Journal of Membrane Science*, 2010. **346**(2): p. 270-279.
68. Li, X., et al., *High-performance SSZ-13 membranes prepared using ball-milled*

- nanosized seeds for carbon dioxide and nitrogen separations from methane.* Chinese Journal of Chemical Engineering, 2020. **28**(5): p. 1285-1292.
69. Wu, S., et al., *An Effective Approach to Synthesize High-Performance SSZ-13 Membranes Using the Steam-Assisted Conversion Method for N₂/CH₄ Separation.* Energy & Fuels, 2020. **34**(12): p. 16502-16511.
 70. Li, Z., et al., *Nitrogen Sorption in a Transition Metal Complex Solution for N₂ Rejection from Methane.* Industrial & Engineering Chemistry Research, 2019. **58**(29): p. 13284-13293.
 71. Gilbertson, J.D., et al., *Coordination chemistry of H₂ and N₂ in aqueous solution. Reactivity and mechanistic studies using trans-FeII (P₂) 2X₂-type complexes (P₂= a chelating, water-solubilizing phosphine).* Inorganic chemistry, 2007. **46**(4): p. 1205-1214.
 72. Friesen, D.T., et al., *Liquid absorbent solutions for separating nitrogen from natural gas.* 2000, Bend Research, Inc.(Bend, OR).
 73. Bomberger, D.C., et al., *Nitrogen removal from natural gas: Phase II.* 1999, Federal Energy Technology Center Morgantown (FETC-MGN), Morgantown, WV
 74. Li, Z., *Separation of Nitrogen from Natural Gas: Conventional and Emerging Technologies.* The University of Western Australia: Perth, Australia, 2018.
 75. Low, W.R. and J. Yao, *Nitrogen rejection system for liquified natural gas.* 2000, Google Patents.
 76. Towler, G. and R. Sinnott, *Chemical engineering design: principles, practice and economics of plant and process design.* 2021: Butterworth-Heinemann.
 77. Turton, R., et al., *Analysis, synthesis and design of chemical processes.* 2008: Pearson Education.

78. Stinn, C. and A. Allanore, *Estimating the capital costs of electrowinning processes*. The Electrochemical Society Interface, 2020. **29**(2): p. 44.
79. Seo, Y. and S. Han, *Economic Evaluation of an Ammonia-Fueled Ammonia Carrier Depending on Methods of Ammonia Fuel Storage*. Energies, 2021. **14**(24): p. 8326.
80. Bedowska-Sojka, B. and J. Górka, *The lithium and oil markets—dependencies and volatility spillovers*. Available at SSRN 4076733.
81. Ibrahim, A. and K. Muammer, *ECONOMIC AND FINANCIAL DEVELOPMENT IMPACTS ON ENERGY CONSUMPTION IN QATAR*. Journal of Management and Economics Research. **20**(1): p. 313-330.